Comenius University in Bratislava

Faculty of Mathematics, Physics and Informatics

Broadband Approach as a Framework for Implementation of Radiative Transfer Scheme with Selective Intermittency: Cost Versus Accuracy Study

Master's Thesis

Bc. Peter Kuma

2015

Comenius University in Bratislava

Faculty of Mathematics, Physics and Informatics

Broadband Approach as a Framework for Implementation of Radiative Transfer Scheme with Selective Intermittency: Cost Versus Accuracy Study

Master's Thesis

Degree Programme: Meteorology and Climatology

Study Field: 1160 Physics

Department: Division of Meteorology and Climatology, Department of Astronomy, Physics of the Earth and Meteorology

Supervisor: Mgr. Ján Mašek, Czech Hydrometeorological Institute, Prague

Bc. Peter Kuma

Bratislava, 2015

44050040

THESIS ASSIGNMENT

Name and Surname:	Bc. Peter Kuma
Study programme:	Meteorology and Climatology (Single degree study, master II. deg., full time form)
Field of Study:	4.1.1. Physics
Type of Thesis:	Diploma Thesis
Language of Thesis:	English
Secondary language:	Slovak

Title: Broadband approach as a framework for implementation of radiative transfer scheme with selective intermittency – cost versus accuracy study

Aim: Propose, implement and test suitable intermittent strategies for ACRANEB scheme, taking into account particularities of shortwave and longwave radiative transfer calculations.

Literature: Ritter B, Geleyn JF. 1992. A comprehensive radiation scheme for numerical weather prediction
models with potential applications in climate simulations. Mon. Weather Rev. 120: 303–325,
doi:10.1175/1520-0493(1992)120 0303:ACRSFN 2.0.CO2.
Geleyn JF, Hollingsworth A. 1979. An economical analytical method for the computation of the
interaction between scattering and line absorption of radiation. Contrib. Atmos. Phys. 52: 1–16.
Mašek J, Geleyn JF, Brožková R, Giot O, Achom HO, Kuma P. 2014. Single interval shortwave
radiation scheme with parameterized optical saturation and spectral overlaps. Manuscript submitted for publication.

Annotation: Clouds are main modulating factor of radiative transfer in the Earth's atmosphere. For realistic numerical weather prediction it is thus desirable to have full feedback between radiative transfer and
quickly evolving clouds. Ideally, this would be achieved by making radiative transfer calculations at every gridpoint and every model timestep. Main obstacle to do this is spectral integration. Extremely
high cost of exact line by line computations prevents their use in numerical weather prediction so that cheaper and somewhat less accurate alternatives must be sought. Traditional solutions are
based either on so called k-distribution method, or on broadband approach. The latter is used also in radiation transfer scheme ACRANEB of model ALADIN, for efficiency reasons having just two
spectral bands – one solar (shortwave) and one thermal (longwave). Even with such broad spectral division it is possible to make the scheme accurate enough by parameterizing optical saturation
of shortwave cloud absorption and spectral overlaps between various radiatively active species. In thermal part, problem of multiple emission sources can be

solved efficiently by using net exchanged rate technique. Still, the cost of radiative transfer calculations with above improvements represents

significant part of model CPU time and it is desirable to reduce it by suitable intermittent strategy. Unlike k-distribution method, broadband approach is especially suitable for implementing selective

intermittency where rapidly varying cloud optical properties are updated at every model timestep, while slowly evolving gaseous transmissions only from time to time. Aim of this work is to propose,

implement and test suitable intermittent strategies for ACRANEB scheme, taking into account particularities of shortwave and longwave radiative transfer calculations.

Comment: Vedúci DP je pracovníkom Českého hydrometeorologického ústavu a je špecialistom na danú problematiku

Keywords: radiation scheme, radiative transfer, numerical weather prediction, net exchange rate

Supervisor: Mgr. Jan Mašek

Department: FMFI.KAFZM - Department of Astronomy, Physics of the Earth and Meteorology

Head of department: prof. RNDr. Peter Moczo, DrSc.

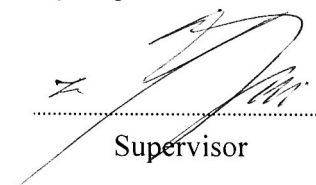**Assigned:** 20.01.2015

Approved: 27.01.2015

prof. RNDr. Milán Lapin, CSc.

Guarantor of Study Programme

....
Student

....
Supervisor

Abstrakt

Abstract

Preface

Contents

Introduction

Radiation schemes (or *radiative transfer codes*) are modules in numerical weather prediction (NWP) models and general circulation models (GCM) responsible for calculation of radiation fluxes in the atmosphere and the ocean. Fluxes are necessary to quantify diabatic heating of atmospheric and oceanic layers. Radiation schemes contribute significantly to the accuracy of NWP models, but also take a large fraction of model run time. Due to the computational complexity of the problem, numerous approximations have to be made (most radically the *two-stream approximation*), but even then it is not possible to perform full radiative transfer calculations in every domain point and every time step in operational settings. Therefore, most models resort to temporal or spatial subsampling of radiative transfer calculations. In the most simple implementation, fluxes calculated by the radiation scheme are kept constant across multiple model time steps, or a single calculation is performed for blocks of neighbouring domain points. More complex implementations interpolate resulting fluxes with respect to changes in temperature profile and the solar zenith angle (Morcrette, Mozdzynski, and Leutbecher 2008). In such a case, the information about temporal or spatial variability is not fully taken into account. The situation is the most serious with cloud cover, which changes rapidly and can have a paramount impact on radiative fluxes. In order to address this issue, the radiation scheme ACRANEB2 was developed, whose aim is to decouple calculation of optical thickness of layers due to gases from one due to clouds and aerosols. The former (more expensive to compute) can then be performed with reduced temporal frequency, while the latter can be performed at every time step. The ACRANEB2 radiation scheme utilises only two spectral intervals: shortwave and longwave. The implementation of temporal subsampling ('intermittency') in the longwave spectrum had already been done, while it was one of the objectives of this work to implement temporal subsampling in the shortwave spectrum.

While in the longwave spectrum gaseous optical thickness can be assumed constant over multiple time steps without a significant loss of accuracy, in the shortwave spectrum it depends on the solar zenith angle, whose change cannot be neglected. Therefore, one of the challenges was to find a suitable interpolation method in order to account for this dependency.

In summary, the objectives of this work were:

1. Find and investigate a suitable time subsampling ('intermittency') method in the shortwave band of the radiation scheme ACRANEB2.

2. Implement the shortwave intermittency method in the code of the scheme.

3. Determine the performance and accuracy of various shortwave intermittency periods in the context of the limited-area NWP model ALADIN.

Chapter 1

Basic Principles of Radiative Transfer

This chapter introduces a number of concepts related to radiative transfer in the Earth's atmosphere, and terms necessary for understanding later chapters unambiguously (as there are many notations in general use). Only the most relevant parts are covered, interested reader is advised to see Petty (2006), Zdunkowski, Trautmann, and Bott (2007), Liou (2002), Thomas and Stamnes (2002) and Goody and Yung (1995) for a more comprehensive development of the radiative transfer theory.

1.1   The Electromagnetic Spectrum

Radiation in the atmosphere can for the most part be represented by electromagnetic (EM) waves. In this context, EM waves can originate from multiple sources, most importantly the Sun, the Earth's surface and atmospheric gases and constituents (clouds and suspended particles such as aerosols). EM waves have different wavelength distribution depending on the temperature of the radiating body through the Planck's law (assuming local thermodynamic equilibrium). Radiation is subject to different levels of absorption and scattering depending on the wavelength when passing through the atmosphere. Traditionally, the EM spectrum is divided into a number of *bands* according to the wavelength (optionally divided further into *subbands*):

- Gamma radiation
- X-rays
- Ultraviolet radiation (UV-C, UV-B, UV-A)
- Visible light
- Infrared radiation (near IR, thermal IR, far IR)
- Microwaves
- Radio waves

Most of them are not of interest to radiative transfer in NWP models and GCM, because they are not present in the atmosphere in energies high enough to influence the heating rates. Specifically, of interest are the UV, visible light and IR bands.

1.1.1   Ultraviolet Radiation

Ultraviolet radiation (UV) is radiated in appreciable amounts only by very hot objects, such as the Sun. It is highly energetic, capable of releasing electrons from atoms (*photoionisation*) and breaking up molecules (*photodissociation*). UV radiation spans wavelengths of 10-400 nm. The UV band is further divided into multiple subbands, of which only the last three are of interest to atmospheric radiative transfer[1]:

- UV-C: 100 nm–280 nm
- UV-B: 280 nm–320 nm
- UV-A: 320 nm–400 nm

Much of UV radiation is absorbed high in the atmosphere (stratosphere and mesosphere) by ozone and oxygen, though UV-A reaches the Earth's surface with little attenuation. UV radiation has to be considered in radiation schemes, because it contributes significantly to heating rates in the stratosphere. It is also important due to its influence on atmospheric chemistry (Chapman reactions).

1.1.2   Visible Light

The visible spectrum comprises wavelengths which humans can perceive with their sight. The likely reason which gave rise to this ability is twofold: (1) this is where the peak power of Sun's radiation is located, and (2) the clear-sky atmosphere is almost transparent in the visible spectrum. Visible light spans the region of about 400–700 nm. In radiation models it has to be considered due to scattering and absorption by air molecules, clouds and aerosols. The only significant source of visible light is the Sun.

1.1.3   Infrared Radiation

Infrared radiation (IR) is emitted by objects of temperatures commonly found in the Earth's environment. The IR band is divided into three additional subbands:

- Near infrared: 700 nm–4.6 μm
- Thermal infrared: 4.6 μm–50 μm

---

[1]The precise choice of boundaries is somewhat arbitrary, and various definitions can be found.

- Far infrared: 50 μm–1 mm

Radiation in the near IR comes mostly from the Sun, while standard temperature objects emit in the thermal and far IR. The atmosphere is rather opaque to the infrared radiation. It is absorbed strongly (but not uniformly) by greenhouse gases: water vapour, CO_2, O_3, CH_4, CO, N_2O, O_2 and CFCs, but also by clouds and aerosols. As it is the main means of radiative energy exchange between the surface, atmospheric layers and space, it is of paramount importance to radiation schemes. Radiation in far infrared (approx. above 100 μm) gradually ceases to be energetically important due to low power emitted at longer wavelengths.

1.1.4 Shortwave and Longwave Spectrum

For the purpose of radiation schemes, it is convenient to adopt two even broader spectral regions – *shortwave* (*solar*) and *longwave* (*thermal*) radiation. Though the choice of precise boundaries is arbitrary, we settle on the following definition:

- Shortwave radiation (UV, visible, near IR): 0.1–4.6 μm
- Longwave radiation (thermal, far IR) : 4.6–100 μm

The justification for this choice is that the Sun emits radiation mostly between 0.1–4.6 μm, while the Earth's surface and atmosphere emit mostly at wavelengths longer than 4.6 μm, with little overlap between the two (Fig. 1.1). This coincidence allows for decoupling of radiative transfer calculations in the two regions. The Sun can, however, be a significant source of radiation even in the thermal IR when considering direct solar radiation or sun glint, important to remote sensing applications (Petty 2006, Sec. 6.3).

1.2 Terms and Definitions

This section summarises terms and definitions of the radiative transfer theory used in later chapters. Especially, there is a number of different notations in use today. We follow those of Petty (2006) due to their clarity.

1.2.1 Frequency, Wavelength and Wavenumber

Frequency of a monochromatic EM wave will be denoted $\tilde{\nu}$. Frequency is related to *wavelength* λ via the speed of light $c = \tilde{\nu}\lambda$. Longer wavelengths are sometimes identified by *wavenumber*[2] $\nu = 1/\lambda$, which is often preferred in the infrared spectrum.

---

[2]Symbols for frequency and wavenumber are sometimes reversed, with $\tilde{\nu}$ denoting wavenumber, and ν frequency.
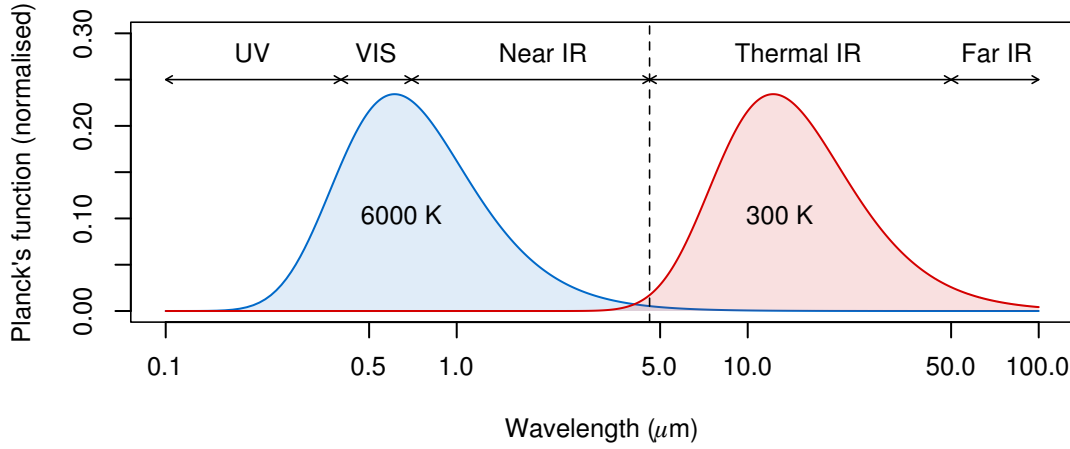
Figure 1.1: Planck's function for the approximate temperature of the Sun (6000 K) and the surface of the Earth (300 K). The small overlap allows for decoupling of radiative transfer calculations in the shortwave and longwave parts of the spectrum. The value is normalised to equal areas. The vertical line show the division at $4.6\,\mu$m (see text). Adapted from Petty 2006.

It is notable that wavenumbers in cm^{-1} can be conveniently converted to wavelengths in μm by the expression $y = 10000/x$, where x is wavenumber and y is wavelength (and vice versa).

1.2.2 Monochromatic Radiance and Radiance

Monochromatic radiance (or *spectral intensity*, *radiant intensity*) is power transmitted by an electromagnetic wave at certain wavelength passing through a unit surface in a particular direction. Monochromatic radiance depends on wavelength λ, position $\mathbf{r}$ and direction given by a unit vector $\hat{\mathbf{\Omega}}$:

$$I_\lambda = I_\lambda(\mathbf{r}, \hat{\mathbf{\Omega}}) \tag{1.1}$$

Monochromatic radiance has units $\text{Wm}^{-3}\text{sr}^{-1}$. When integrated over an interval of wavelenths, we get *radiance*:

$$I = \int_{\Delta\lambda} I_\lambda \mathrm{d}\lambda = I(\mathbf{r}, \hat{\mathbf{\Omega}}) \tag{1.2}$$

Radiance has units $\text{Wm}^{-2}\text{sr}^{-1}$. As *monochromatic radiance* will be discussed frequently in this text, we will call it simply 'radiance' and denote I and state explicitly if *radiance* is considered by calling it *narrow-band* or *broadband radiance*. We will also assume implicit dependence on $\mathbf{r}$ in order to make equations more readable.

1.2.3   Flux Density and Net Flux Density

Flux density is radiance integrated over a hemisphere. In plane parallel geometry, depending on the hemisphere we speak of *upward* or *downward* flux density:

$$F^\uparrow = \int_\uparrow I(\hat{\boldsymbol{\Omega}}) \hat{\mathbf{n}} \cdot \hat{\boldsymbol{\Omega}} \mathrm{d}\omega \tag{1.3}$$

$$F^\downarrow = \int_\downarrow I(\hat{\boldsymbol{\Omega}}) \hat{\mathbf{n}} \cdot \hat{\boldsymbol{\Omega}} \mathrm{d}\omega \tag{1.4}$$

where $\int_\uparrow$, $\int_\downarrow$ represent integration over the top and bottom hemisphere (resp.).

Net flux density is the difference between the upward and downward flux densities:

$$F^{\mathrm{net}} = F^\uparrow - F^\downarrow \tag{1.5}$$

1.2.4   Mass and Volume Absorption/Extinction Coefficients

The fractional loss in radiance $\mathrm{d}I$ due to absorption over a path $\mathrm{d}s$ can be expressed with the *volume absorption coefficient* β_a:

$$\mathrm{d}I = -I\beta_a \mathrm{d}s \tag{1.6}$$

In gases, this process depends only on the amount of absorber per unit area along the path $\mathrm{d}u = \rho \mathrm{d}s$, and 1.6 can be expresses equivalently with the *mass absorption coefficient* $k_a = \beta_a/\rho$:

$$\mathrm{d}I = -I k_a \mathrm{d}u \tag{1.7}$$

Both k_a and β_a depend on the type of absorber and are functions of wavelength. In addition, they may depend on pressure and temperature, which determine absorption line properties:

$$k_a = k_{a,\lambda,\mathrm{absorber}}(\mathbf{r}, p, T), \tag{1.8}$$

$$\beta_a = \beta_{a,\lambda,\mathrm{absorber}}(\mathbf{r}, p, T). \tag{1.9}$$

Note that while β_a depends on the absorber density ρ, k_a generally does not.

Volume extinction coefficient β_e and *mass extinction coefficient* k_e are defined in the same manner, but here we consider total loss of radiance due to absorption and scattering to all directions, as discussed in the section on radiative transfer equation (Sec. 1.3).

1.2.5 Emissivity and Albedo

1.2.6 Optical Path, Optical Depth, Optical Thickness and Transmittance

Optical path τ is defined as the integral of volume extinction coefficient over a finite path through an absorbing medium:

$$\tau(s_1, s_2) \equiv \int_{s_1}^{s_2} \beta_e(s)\mathrm{d}s \tag{1.10}$$

Optical depth is denoted by the same symbol τ, and is the vertical optical path between the top of the atmosphere and a height z:

$$\tau(z) \equiv \int_{z}^{\infty} \beta_e(z')\mathrm{d}z \tag{1.11}$$

Optical thickness τ (again denoted by the same symbol) is the vertical optical path between two levels z_1 and z_2:

$$\tau \equiv \tau(z_2) - \tau(z_1) \tag{1.12}$$

Transmittance (or *transmissivity*) t is the fraction of radiance passing through a layer of absorber. In a non-scattering medium with no sources, it is related to optical thickness τ by:

$$t = \exp(-\tau) \tag{1.13}$$

1.2.7 Heating Rate

Heating rate of a layer of atmosphere by radiation is given by the difference of net flux density between its top and bottom interfaces, which is a consequence of energy conservation – the energy is transferred from radiation to air molecules and airborne particles in the layer.

1.3   The Radiative Transfer Equation

Fundamentally, radiative transfer is governed by the Maxwell equations and quantum mechanical principles. However, it is often not necessary to be concerned with the details of the electromagnetic field in the context of energy budget calculations, perhaps with the exception of Mie theory of scattering.

There are three energetically important processes in which radiation interacts with matter in the atmosphere: *scattering*, *absorption* and *emission*. Put together they form the radiative transfer equation.

1.3.1   Scattering

Scattering of radiation occurs when a charged particle is made to oscillate in a passing electromagnetic wave, generating new electromagnetic radiation, which modifies the original field. There is no net exchange of energy between the particle and the field at the end of the process.

We will define the *scattering phase function* to be a function of two unit vectors $\hat{\mathbf{\Omega}}'$ and $\hat{\mathbf{\Omega}}$ (in addition to the implicit dependence on the position $\mathbf{r}$), giving the fraction of radiance scattered from the direction of $\hat{\mathbf{\Omega}}'$ in the of $\hat{\mathbf{\Omega}}$:

$$p = p(\hat{\mathbf{\Omega}}', \hat{\mathbf{\Omega}}) \tag{1.14}$$

subject to normalisation condition (energy conservation):

$$\frac{1}{4\pi} \int_{4\pi} p(\hat{\mathbf{\Omega}}', \hat{\mathbf{\Omega}}) \mathrm{d}\omega = 1 \tag{1.15}$$

In the presence of scattering only, the differential change in radiance is:

$$\mathrm{d}I(\hat{\mathbf{\Omega}}) = -I(\hat{\mathbf{\Omega}})\beta_s \mathrm{d}s + \beta_s \mathrm{d}s \frac{1}{4\pi} \int_{4\pi} p(\hat{\mathbf{\Omega}}', \hat{\mathbf{\Omega}}) I(\hat{\mathbf{\Omega}}') \mathrm{d}\omega' \tag{1.16}$$

i.e. the change in radiance is equal to the amount removed by scattering in all directions, compensated by radiation scattered into the direction of $\hat{\mathbf{\Omega}}$ from all other directions.

1.3.2 Absorption and Beer's Law

Radiation passing through the atmosphere can be absorbed by air molecules and larger objects present in the atmosphere (such as cloud droplets and aerosol particles). In the process, the energy of a photon is absorbed to cause an electronic, vibrational or rotational transition in an atom or molecule. This can be later turned into kinetic energy, causing an increase in temperature. The photon is lost in the process, and radiance is reduced by the corresponding amount of energy.

The influence of absorption on radiance is described by the volume absorption coefficient β_a (discussed in Sec. 1.2.4):

$$\mathrm{d}I = -I\beta_a\mathrm{d}s \tag{1.17}$$

If we integrate this equation over a finite path, assuming β_a is constant, we get the *Beer's law*:

$$I(s) = I(0)\exp(-\beta_a s) \tag{1.18}$$

i.e. monochromatic radiance falls of exponentially in a homogeneous, absorbing, non-scattering medium. The same relationship applies to absorbers whose volume absorption coefficient is independent of wavelength (over the interval of interest), also called *gray bodies*[3].

1.3.3 Emission

Thermal emission of radiation by a body is bounded by the *Planck's law*:

$$B_\lambda(T) = \frac{2hc^2}{\lambda^5(e^{hc/k_B\lambda T} - 1)} \tag{1.19}$$

where $B_\lambda(T)$ is radiance emitted by a *blackbody* with temperature T. Bodies which are not perfectly black emit less radiation according to their *emissivity*. In the case of bodies which are not a surface, such the air, the volume absorption coefficient β_a has the role of emissivity, and the true radiance emitted by such a body over a path $\mathrm{d}s$ in the direction of $\mathrm{d}s$ is:

---

[3]In analogy to visible light, in which they appear gray.

$$\mathrm{d}I_{\mathrm{emit}} = \beta_a B \mathrm{d}s \qquad (1.20)$$

We do not need to introduce any volume emission coefficient, as by the *Kirchhoff's law* under the condition of a local thermodynamic equilibrium (LTE) absorptivity is equal to emissivity. This condition is satisfied in parts of the atmosphere where radiative energy budget calculations are important to NWP (troposphere and stratosphere).

1.3.4 Radiative Transfer Equation

The full form of the *radiative transfer equation* (RTE) combines the contributions of extinction, emission and scattering in a single equation:

$$\mathrm{d}I = -\mathrm{d}I_{\mathrm{ext}} + \mathrm{d}I_{\mathrm{emit}} + \mathrm{d}I_{\mathrm{scat}}$$

$$\mathrm{d}I(\hat{\boldsymbol{\Omega}}) = -\beta_{\mathrm{e}}\mathrm{d}s I(\hat{\boldsymbol{\Omega}}) + \beta_{\mathrm{a}}\mathrm{d}s B(\hat{\boldsymbol{\Omega}}) + \beta_{\mathrm{s}}\mathrm{d}s \frac{1}{4\pi} \int_{4\pi} p(\hat{\boldsymbol{\Omega}}', \hat{\boldsymbol{\Omega}}) I(\hat{\boldsymbol{\Omega}}') \hat{\mathbf{n}} \cdot \mathrm{d}\hat{\boldsymbol{\Omega}}' \qquad (1.21)$$

where $\mathrm{d}s$ is in the direction of $\hat{\boldsymbol{\Omega}}$.

It is the purpose of radiation schemes to find an approximate solution to the radiative transfer equation. Before this task becomes computationally feasible in operational NWP models, the equation has to be simplified in a number ways, as discussed in Chapter 3.

Chapter 2

Radiatively Active Gases

Radiation passing through the Earth's atmosphere is modified by the processes of absorption and scattering. Both of these processes are wavelength-dependent, but while scattering is determined by Rayleigh scattering, Mie theory and geometric optics, in order to fully determine absorption we need to know the specific absorption lines of radiatively active gases.

Absorption spectrum of gas molecules can have immensely complicated structure, and one needs a very large amount of information to describe the structure fully. Additionally, smoothing the curve by averaging out the details is of little use in calculation of transmittance due to saturation at wavelengths where absorption is strongest (line centres). This chapter discusses the physical basis of absorption by gases, while Chapter 3 introduces approaches to overcoming this problem.

Spectroscopic data of absorption lines of gases are available from spectroscopic databases. One of the most comprehensive databases is HITRAN[1] (Rothman et al. 2009). For gases where continuum absorption is important, one needs to use an additional model such as MT_CKD produced by AER (E. J. Mlawer et al. 2012), which includes continuum absorption of water vapour, nitrogen, oxygen, carbon dioxide and ozone.

2.1 Types of Transitions

Gases can absorb and emit radiation only in the vicinity of precise wavelengths – absorption lines, due to restrictions imposed by the quantum theory. In particular, the energy has to match one of the allowed *electronic*, *vibrational* or *rotational* transitions, up to a perturbation due to a collision (pressure broadening) and velocity (Doppler broadening).

---

[1]https://www.cfa.harvard.edu/hitran/. The HITRAN database can be browsed conveniently at 'HITRAN on the Web' (http://hitran.iao.ru).

Electronic transitions are the most energetic, associated with electrons transitioning into other energy levels within atoms, or breaking free entirely, in which case there is a continuum absorption, because any extra energy can transform into kinetic energy of the escaping electron. Electronic transitions are mostly responsible for absorption in the high-frequency part of the spectrum below 300 nm.

Vibrational transitions are less energetic than electronic, but more energetic than rotational transitions. They are due to transitions between vibrational modes of multi-atomic molecules. Not all molecules have vibrational transitions. They are subject to the condition that EM wave has the be able to exert force on the atoms, for which the molecule needs to have a dipole moment (be polarised). Notably, the most abundant atmospheric gas N_2 does not have a dipole moment, and therefore does not posses vibrational modes[2]. The number of vibrational modes generally depend on the number of atoms in the molecule.

Rotational transitions are caused transitions between rotational modes of multi-atomic molecules. Rotational transitions are the least energetic. As transitions can occur together, and because they are much less energetic than vibrational transitions, they combine to produce vibrational bands with fine structure, centred at a particular wavelength of a vibrational transition. Not all molecules have rotational transitions. In particular, the EM wave has to be able to exert torque on the molecule. Especially, it needs to have a dipole moment, or an intrinsic magnetic moment (as is the case with O_2).

2.2   Shortwave Absorption

In the shortwave spectrum, solar radiation is absorbed significantly (in terms of the energy budget) by the following gases:

- Water vapour (H_2O)
- Ozone (O_3)
- Carbon dioxide (CO_2)
- Oxygen (O_2, O)
- Methane (CH_4)
- Nitrous oxide (N_2O)

Solar absorption is the greatest in the high-frequency range. In particular, gamma radiation, X-rays and UV-C are almost entirely absorbed early in their travel through the atmosphere, mostly by oxygen and ozone. As such, and because they constitute only a

---

[2]However, vibrational transitions sometimes can occur even in these molecules if they are affected by an EM wave at the time when there is a collision with another molecule of air, temporarily creating a dipole. Some molecules also form compounds in the form of dimers or multimers, in which case new modes may become available.
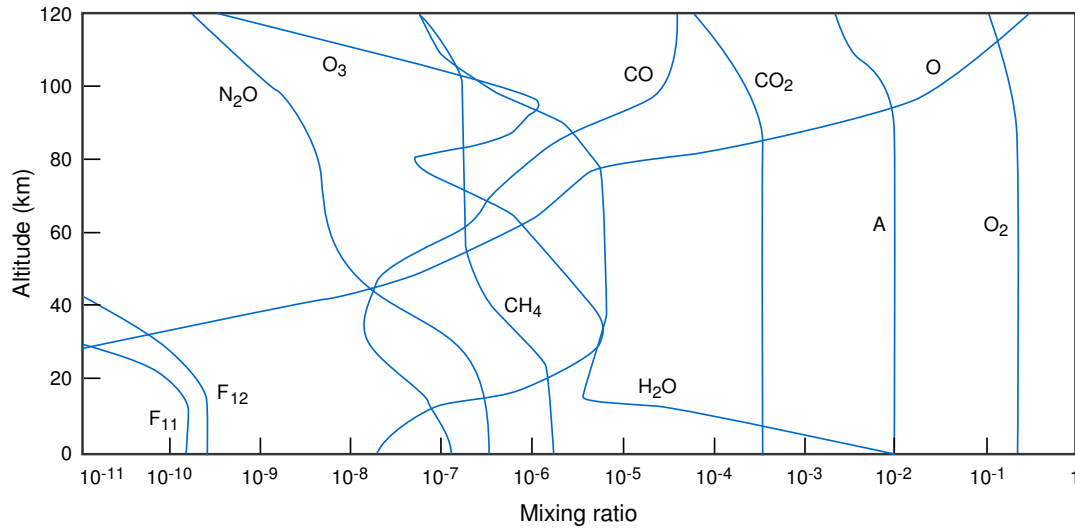
Figure 2.1: Atmospheric composition. Vertical profiles of mixing ratio of selected species at equinox. Adapted from Goody and Yung 1995. After Allen et. al. (1981, 1984).

small contribution of energy to low and mid-altitudes, they are of little concern to NWP. In the UV spectrum, radiation is strongly absorbed by bands of ozone (Hartley, Huggins bands), important in the stratosphere. In the visible spectrum, clear-sky atmosphere is almost transparent, with a few weaker bands of ozone (Chappius band) and oxygen ('red bands'). In the near IR, radiation is again absorbed strongly by multiple bands of water vapour, but also carbon dioxide, oxygen ('infrared bands'), methane and nitrous oxide. Both absorption in the visible and near IR spectrum has to be accounted for for an accurate radiative transfer prediction in NWP. The importance of absorption bands in the shortwave spectrum is given not only by their strength (absorption cross section) and concentration of the absorbing gas, but also by the solar spectrum, which falls off quickly below about $0.2\ \mu$m, and above $3\ \mu$m.

Absorption bands of gases important to solar absorption (discussed in the following sections) can be seen in Figure 2.2, Figure 2.1 shows concentration of gases in the atmosphere, and Figure 2.3 shows heating rates attributed to the major shortwave absorbing atmospheric gases.

2.2.1 Water Vapour

Water vapour is the most important shortwave absorption gas. It is abundant in the troposphere, where it falls off sharply with height due to condensation. It is also highly spatially and temporally variable.

Water vapour absorbs radiation in a number of bands in the shortwave spectrum, most importantly in the near IR centred at $2.7\ \mu$m (χ), $1.87\ \mu$m (Ω), $1.38\ \mu$m (ψ), $1.1\ \mu$m (φ),
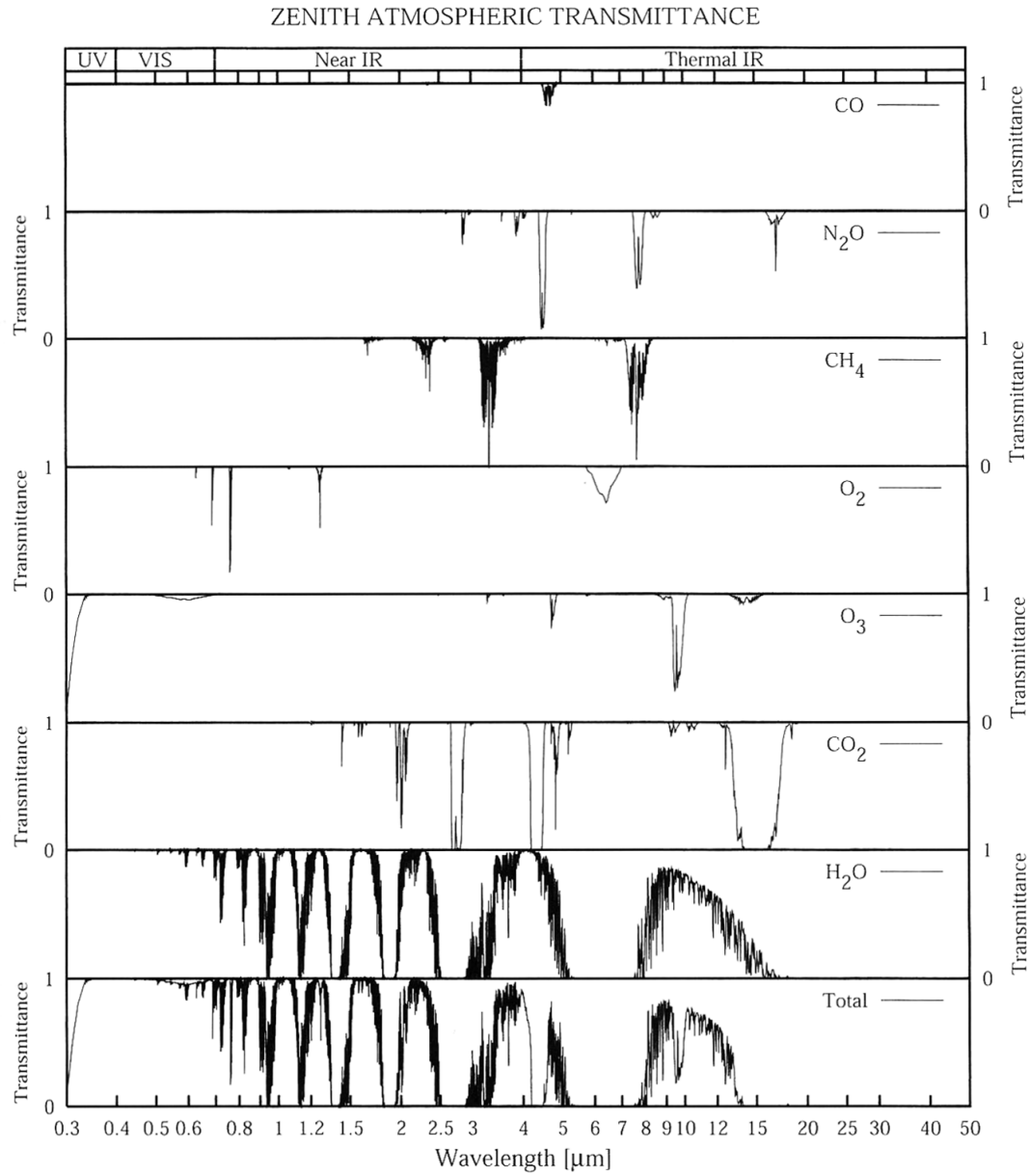
Figure 2.2: Zenith clear-sky transmittance in midlatitude summer attributed to gases. Panels show absorption contribution of atmospheric gases. Molecular scattering is not considered. Adopted from Petty 2006.
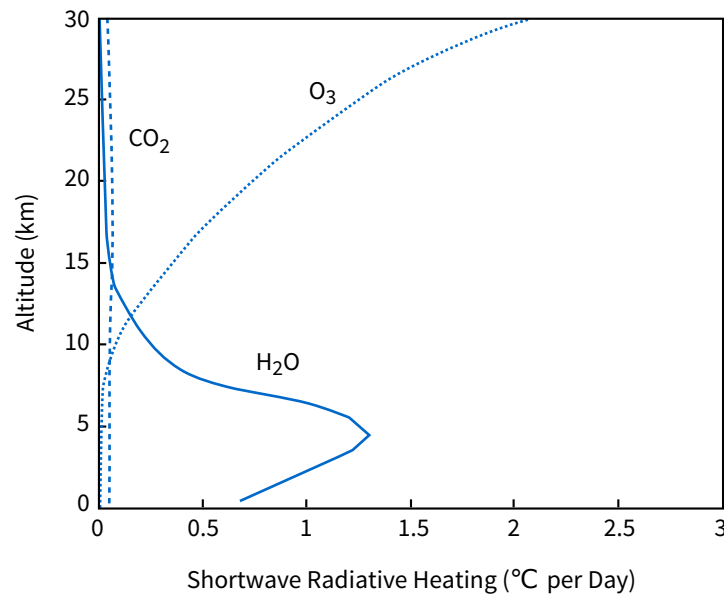
Figure 2.3: Shortwave heating rate profile due absorption by atmospheric gases. This profile was derived for cloud-free tropical conditions and solar zenith angle of 30°. Adapted from Petty 2006. Figure courtesy of S. Ackerman.

$0.94~\mu$m (ρ, σ, τ), $0.82~\mu$m and $0.72~\mu$m (Goody and Yung 1995; Liou 2002). All of these are important to solar heating in the atmosphere. There are also absorption lines in the visible spectrum, but are said not to contribute significantly to heating rates (Liou 2002).

2.2.2 Ozone

Ozone (O_3) exhibits a number of bands in the shortwave spectrum: *Hartley bands*, *Huggins bands* and *Chappuis bands* (Figure 2.4). All of them are in the form of continuum due to photodissociation, although Huggins bands have a more irregular structure. Of the three, Hartley bands are the strongest. They cover the region of 240–310 nm. Because of their strength, they absorb most incident solar radiation in the mesosphere and stratosphere. Huggins bands cover the region of 310–340 nm. Although Chappuis bands are the weakest of the three, they are important for atmospheric absorption, because they lie in the region of 450–750 nm, where solar radiation is the strongest. Their principal location of absorption is in the troposphere.

2.2.3 Carbon Dioxide

Carbon dioxide (CO_2) is mostly active in the longwave spectrum, but exhibits a number of bands in the shortwave as well. The strongest is centred at $2.7~\mu$m, and a number of

Absorption by 300 DU of O3, S0 = 1361 W/m², T = 253 K
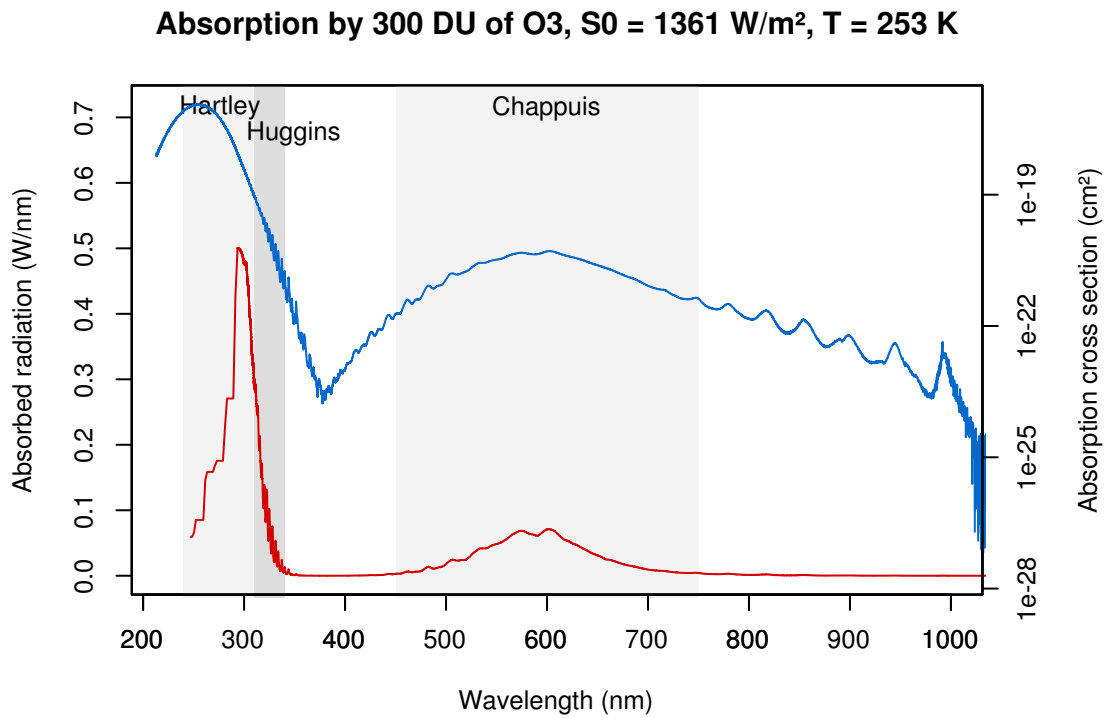
Figure 2.4: Ozone shortwave absorption. Absorbed solar radiation (**red**) and absorption cross section (**blue**) of O_3. Indicated are approximate regions of the Hartley, Huggins and Chappuis absorption bands. Data from Serdyuchenko et al. 2013.

Figure 2.5: Oxygen shortwave absorption. Absorption cross section of oxygen $^{16}O^{16}O$ in the ultraviolet band. Adopted from Goody and Yung 1995. After Brasseur and Solomon (1984).
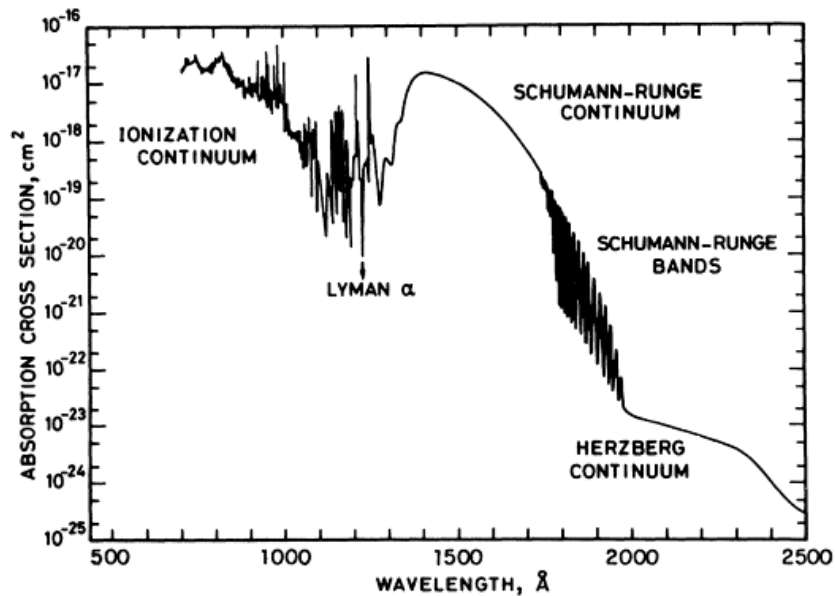
weaker bands are at $2.0\ \mu\mathrm{m}$, $1.6\ \mu\mathrm{m}$, $1.4\ \mu\mathrm{m}$ (Liou 2002).

2.2.4 Oxygen

Oxygen (O_2, O) absorption happens mostly in the ultraviolet, where it is associated with electronic transitions. High-frequency UV absorption cross section is shown in Figure 2.5. The strength of this absorption means that little UV radiation penetrates the atmosphere in this region.

Even though O_2 is a homonuclear diatomic molecule with no electric dipole moment, it has a permanent magnetic moment, enabling rotational transitions to occur.

Outside of the UV band, oxygen absorbs in the *red* and *infrared* 'atmospheric' bands (Goody and Yung 1995). They are associated with the $\mathrm{a} \leftarrow \mathrm{X}$ (resp. $\mathrm{b} \leftarrow \mathrm{X}$) electronic transition in combination with vibrational-rotational transitions. The red bands comprise band A centred at 762 nm, band B at 688 nm, and band γ at 628 nm. Infrared bands are centred at $1.58\ \mu\mathrm{m}$, $1.27\ \mu\mathrm{m}$ and $1.06\ \mu\mathrm{m}$. Although relatively sparse, the red bands are important to the tropospheric energy budget, because they they are located at the peak of the solar spectrum (Liou 2002).

Oxygen molecules are known to form dimers with some other atmospheric constituents, notably $O_2.N_2$ and O_4. These have additional bands believed to contribute roughly $1\ \mathrm{Wm}^{-2}$ to the total atmospheric absorption (Solomon et al. 1998).

2.2.5 Methane

Methane (CH_4) is not active in the visible spectrum, but has a number of bands in the near IR clustered between 3 and $4\ \mu\mathrm{m}$ (3.38, 3.53, 3.26), 2 and $2.5\ \mu\mathrm{m}$ (2.37, 2.30, 2.20) and at $1.66\ \mu\mathrm{m}$.

2.2.6 Nitrous Oxide

Nitrous oxide (N_2O) has a few absorption bands in the near IR spectrum important to solar absorption: $4.06\ \mu\mathrm{m}$, $3.90\ \mu\mathrm{m}$, $2.97\ \mu\mathrm{m}$ and $2.87\ \mu\mathrm{m}$ (Liou 2002).

2.3 Absorption Lines

Atmospheric gases do not absorb and emit radiation at exact wavelengths. Instead, absorption lines are spread out over a range of frequencies by three types of processes:

- Natural broadening
- Doppler broadening

- Pressure broadening

Natural broadening occurs due to quantum mechanical effects and is very weak compared to the other two. Therefore, it has little importance to atmospheric radiative transfer.

Doppler broadening occurs due to Doppler shift in frequency as observed by a moving molecule. It has a normal (Gaussian) shape. Doppler broadening is the dominant form of broadening in the upper atmosphere.

Pressure broadening is the most important type of broadening to atmospheric radiative transfer. It occurs due to collisions between molecules, which impose a finite time limit on absorption and emission of a monochromatic EM wave.

Effects of all three types of broadening are combined together to produce a characteristic *line shape* of an absorption line. Line shape is defined as function $f(\nu)$, such that the absorption coefficient of an isolated line is:

$$k_\nu = Sf(\nu) \tag{2.1}$$

where S is the line strength. The shape function itself is normalised to unity:

$$\int_0^\infty f(\nu)\mathrm{d}\nu = 1 \tag{2.2}$$

Pressure broadening is described by the *Lorentz line shape*, Doppler broadening by the *Doppler line shape*, and together they are described by the *Voigt line shape*.

2.3.1   Pressure Broadening

Molecules in the atmosphere collide with each other at very high frequency. Every time a collision happens any absorption or emission process under way is interrupted. When a stimulation by a monochromatic wave is limited to a finite amount of time, this is equivalent to stimulation by a range of frequencies, which can be reconstructed by performing Fourier transform on the amplitude function. By taking into account the statistical distribution of time between collisions (Poisson distribution), we can calculate the relative probability of absorption/emission at every frequency. The derivation is carried out in e.g. Zdunkowski, Trautmann, and Bott (2007), here we show only the important result – the *Lorentz line shape*:

$$f(\nu) = \frac{\alpha}{\pi[(\nu - \nu_0)^2 + \alpha^2]} \tag{2.3}$$

where ν_0 is the line centre and α is the line *half-width*. It should be noted that this only applies to high enough wavenumbers (compared to the half-width), but this is only concern to microwaves and longer wavelengths.

The half-width α depends on the mean time between collision, which can be expressed in terms of pressure and temperature as:

$$\alpha = \alpha_0 \frac{p}{p_0} \left(\frac{T_0}{T}\right)^n \tag{2.4}$$

where α_0 is the half-width at reference pressure and temperature p_0, T_0, and n is an empirically determined exponent, which depends on the type of the molecule.

It has to be said that the theory outlined above (*Michelson-Lorentz theory*) does not hold exactly (Goody and Yung 1995). Especially, collisions themselves are not instantaneous, but take finite amount of time. Perhaps most importantly, the Lorentz line shape is insufficient in describing the line shape in far-wings of lines, which contribute very significantly to absorption in spectral windows, where there is no other absorption, and a far-wings of many distant lines add up.

2.3.2 Equivalent Width

The *equivalent width* of a line is the spectral width of a perfectly opaque square line which would absorb the same about of radiation. For a line of any shape it can be calculated as:

$$W = \int_0^\infty (1 - e^{-k_\nu u}) d\nu \tag{2.5}$$

As such, it is not an intrinsic property of a line, but depends on the mass path u.

2.3.3 Weak Line Limit

It is useful to consider the special case when the amount of absorber is relatively small. The equation of equivalent width can then be linearised to give a simplified equation:

$$W = \int_0^\infty (1 - e^{-k_\nu u}) d\nu \approx \int_0^\infty (1 - (1 - k_\nu u)) d\nu = \int_0^\infty S f(\nu) u \, d\nu = Su \tag{2.6}$$

In the weak line limit, the absorption by a single line is independent from line shape, and it is linear with mass path.

2.3.4   Strong Line Limit

The equivalent width of an arbitrary Lorentz line is:

$$W = \int_0^\infty \left(1 - \exp\left(-\frac{Su\alpha}{\pi[(\nu - \nu_0)^2 + \alpha^2]} \right) \right) d\nu \tag{2.7}$$

If the lower integration limit is extended to -∞, and u is substituted by non-dimensional mass path $\tilde{u} = Su/(2\pi\alpha)$, the integration can be performed analytically to give:

$$W = 2\pi\alpha L(\tilde{u}) \tag{2.8}$$

where L is the Ladenburg-Reiche function, defined in terms of the modified Bessel function of the first kind:

$$L(\tilde{u}) = \tilde{u}e^{-\tilde{u}}[I_0(\tilde{u}) + I_1(\tilde{u})] \tag{2.9}$$

Using this analytic form, it can be shown that for large mass path, equivalent width approaches:

$$W \approx 2\sqrt{S\alpha u} \tag{2.10}$$

This is the *strong line limit*, when absorption by a single line grows in proportion to the square root of mass path $\sqrt{u}$.

The absorption by a single line starts off linearly, but with increasing absorber amount the monochromatic radiance near the line centre becomes depleted, and the rate of absorption is reduced to sub-linear (square-root) regime. This can be thought of as *saturation* of absorption, and is similar in the context of multiple overlapping absorption lines.

2.4   Continuum

Gases absorb radiation in discrete absorption lines approximated by the Lorentz or Voigt line shape. However, in some molecules there are parts of the spectrum where the absorption coefficient varies relatively little with wavelength, without apparent association with absorption lines. Typically, this *continuum absoprtion* occurs in connection with photoionization and photodissociation, when the extra energy is consumed by kinetic energy of the escaping electron, resp. broken-up molecules. These processes are mostly confined to the ultraviolet part of the spectrum, because of the high energies required. In addition to photoionisation and photodissociation, there are other less well-explained sources of continuum absorption at lower frequencies due to:

- Far-wings of absorption lines
- Collision induced absorption
- Absorption by dimers and multimers

Even though continuum absorption is generally weak compared to line absorption (with the exception of UV), it is still of great importance, because it covers large parts of the spectrum, often in places where there is absence of line absorption (*atmospheric windows*).

Water vapour is the most important source of continuum for the energy budget, responsible for as much as 40 % of longwave radiative cooling (E. J. Mlawer et al. 2012). The continuum is mostly of two origins: far wings of lines and collision between molecules (self and foreign continuum).

Chapter 3

Approximate Solutions of the Radiative Transfer Equation

In order to make solution of the radiative transfer equation computationally feasible, and number of approximations are commonly taken in operational radiation schemes.

3.1 Plane Parallel Approximation

The atmosphere forms a thin envelope of the Earth with horizontal scales much pronounced relative to vertical scales. Factors influencing radiative transfer include gaseous concentrations, clouds, air and surface temperature variation. Perhaps with the exception of cumulus clouds, all of these change slowly in the horizontal direction, and we can simplify the calculations if we treat them as constant over relatively large areas. In NWP models, this is commonly done by dividing the computational domain into a grid and applying *plane parallel approximation* within each grid cell. In plane parallel approximation, the dependence of quantities on (x,y) coordinates is dropped. Quantities are therefore functions of a single spatial coordinate z, or an equivalent vertical coordinate.

Alternative to the plane parallel approximation is a full three-dimensional treatment of radiation, generally performed by Monte Carlo simulation. This is however too computationally expensive to be done in today NWP models.

3.1.1 Layers

In the plane-parallel approximation the atmosphere is often discretised into *layers*, in which quantities such as temperature and gaseous concentrations are constant. Layer interfaces (boundaries) are defined by fixed vertical coordinates, usually pressure levels.

In the following text we assume that layers are numbered from top to bottom by integer number k, where $k = 1$ is the uppermost layer, and $k = N$ the layer just above the surface. Some quantities, such as fluxes, need to be determined on layer interfaces. The layer interface corresponding to the top of the atmosphere will be numbered $k = 0$, increasing down to the atmosphere-surface interface $k = N$.

3.1.2   Radiative Transfer Equation in Plane Parallel Approximation

In the plane parallel approximation, the radiative transfer equation can be expressed in terms of a single spatial coordinate z. Defining $\mu \equiv \cos(\theta)$[1] and noting that $\mathrm{d}s = \mathrm{d}z/\mu$, (1.21) transforms to:

$$\mu\frac{\mathrm{d}I(\hat{\mathbf{\Omega}})}{\mathrm{d}z} = -\beta_{\mathrm{e}}I(\hat{\mathbf{\Omega}}) + \beta_{\mathrm{a}}B(\hat{\mathbf{\Omega}}) + \frac{\beta_{\mathrm{s}}}{4\pi}\int_{4\pi}p(\hat{\mathbf{\Omega}}', \hat{\mathbf{\Omega}})I(\hat{\mathbf{\Omega}}')\mathrm{d}\omega' \qquad (3.1)$$

More conveniently, we can use *optical depth* $\mathrm{d}\tau = -\beta_{\mathrm{e}}\mathrm{d}z$ as a vertical coordinate, and normalise by β_e:

$$\mu\frac{\mathrm{d}I(\hat{\mathbf{\Omega}})}{\mathrm{d}\tau} = I(\hat{\mathbf{\Omega}}) - (1 - \tilde{\omega})B(\hat{\mathbf{\Omega}}) - \frac{\tilde{\omega}}{4\pi}\int_{4\pi}p(\hat{\mathbf{\Omega}}', \hat{\mathbf{\Omega}})I(\hat{\mathbf{\Omega}}')\mathrm{d}\omega' \qquad (3.2)$$

where $\tilde{\omega} \equiv \beta_{\mathrm{s}}/\beta_{\mathrm{e}}$ is the *single scatter albedo*. This is the *radiative transfer equation in plane parallel atmosphere*.

The geometry of the problem is shown schematically in Figure 5.1.

3.2   Delta-Two Stream Approximation

In the δ-*two stream approximation* radiance is assumed to be constant over hemispheres, with the exception of a peak[2] from direct solar radiation (if present). The peak is treated separately in order to preserve good accuracy, as direct radiance can be orders of magnitude greater than diffuse radiance. There is no azimuthal or zenith dependence of diffuse radiance, and the total radiance is the sum of diffuse and direct radiance:

---

[1]As noted by Petty (2006), p. 325, some authors use the definition $\mu_0 \equiv |\cos(\theta)|$. Here, we use $\mu_0 \equiv \cos(\theta)$ as it leads to more straightforward equations in this situation.

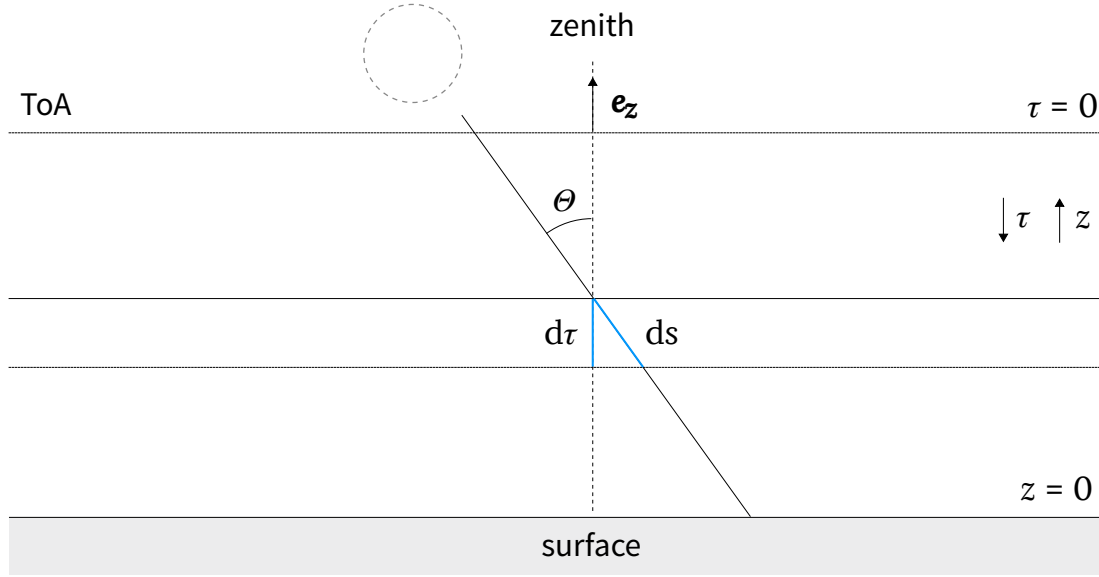[2]Not to be confused with the forward peak of the phase function.

Figure 3.1: Geometry of the plane parallel approximation. Arrows indicate the direction of increase of the optical depth τ and the vertical coordinate z.

$$I = I_{\mathrm{diff}} + I_{\mathrm{dir}} \tag{3.3}$$

$$I_{\mathrm{diff}}(\mu, \phi) = \begin{cases} I^{\uparrow} & \mu > 0 \\ I^{\downarrow} & \mu < 0 \end{cases} \tag{3.4}$$

where $I^{\uparrow}$ and $I^{\downarrow}$ are upward and downward radiance. $I^{\uparrow}$ and $I^{\downarrow}$ are functions of position only. This allows integration over each hemisphere to be performed in a closed-form to get upward, downward and solar flux density (notice that for convenience we redefine $F^{\uparrow}$ and $F^{\downarrow}$ to be the diffuse flux only, in contrast to Sec. 1.2.3):

$$F^{\uparrow} \equiv \int_{\uparrow} I_{\mathrm{diff}}(\hat{\boldsymbol{\Omega}})\hat{\mathbf{n}} \cdot \hat{\boldsymbol{\Omega}} \, \mathrm{d}\omega = \int_0^{2\pi} \int_0^1 I_{\mathrm{diff}}(\mu, \varphi)\mu \, \mathrm{d}\mu \mathrm{d}\varphi = \pi I^{\uparrow} \tag{3.5}$$

$$F^{\downarrow} \equiv \int_{\downarrow} I_{\mathrm{diff}}(\hat{\boldsymbol{\Omega}})\hat{\mathbf{n}} \cdot \hat{\boldsymbol{\Omega}} \, \mathrm{d}\omega = \pi I^{\downarrow} \tag{3.6}$$

$$S \equiv \int_{4\pi} I_{\mathrm{dir}}(\hat{\boldsymbol{\Omega}})\hat{\mathbf{n}} \cdot \hat{\boldsymbol{\Omega}} \, \mathrm{d}\omega \tag{3.7}$$

Therefore, radiance is fully represented by two diffuse flux densities (upward and downward) and the flux density of direct (solar) radiation. The upward and downward diffuse flux densities will be denoted as $F_{\uparrow}$ and $F_{\downarrow}$, and the flux density of solar radiation as S. Here, we assume that S is coming from the Sun, and so always has a direction somewhere in the bottom hemisphere.

3.2.1 Radiative Transfer Equation of Direct Radiation

Let us now consider the plane parallel radiative transfer equation (3.2). In our decomposition into diffuse and direct radiation this equation now does not have a unique solution, as I_{diff} and I_{dir} overlap at the angle of the direct radiation, and we cannot tell how much of the value of the right hand side is allotted to the change in diffuse radiation $\text{d}I_{\text{diff}}$ and direct radiation $\text{d}I_{\text{dir}}$ on the left hand side. Therefore, we postulate that the change in direct radiation is only due to extinction of direct radiation and scattering of direct radiation in the direction of the forward δ peak of the phase function:

$$\mu\frac{\text{d}I_{\text{dir}}(\hat{\boldsymbol{\Omega}})}{\text{d}\tau} \equiv I_{\text{dir}}(\hat{\boldsymbol{\Omega}}) - \frac{\tilde{\omega}}{4\pi}\int_\delta p(\hat{\boldsymbol{\Omega}}, \hat{\boldsymbol{\Omega}}')I_{\text{dir}}(\hat{\boldsymbol{\Omega}})\text{d}\omega' \tag{3.8}$$

To simplify further, we define that the peak of solar radiance has the shape of the Dirac δ function[3]:

$$I_{\text{dir}}(\hat{\boldsymbol{\Omega}}) = \frac{S}{\mu_0}\delta(\hat{\boldsymbol{\Omega}}\cdot\hat{\boldsymbol{\Omega}}_0 - 1) \tag{3.9}$$

where $\hat{\boldsymbol{\Omega}}_0$ is a unit vector in the direction of the radiation, and $\mu_0 = -\hat{\boldsymbol{\Omega}}_0\cdot\hat{\mathbf{e}}_{\mathbf{z}}$ the corresponding cosine of the zenith angle, and express the phase function approximately as:

$$p(\hat{\boldsymbol{\Omega}}', \hat{\boldsymbol{\Omega}}) \approx (1 - f)p'(\hat{\boldsymbol{\Omega}}', \hat{\boldsymbol{\Omega}}) + 2f\delta(\hat{\boldsymbol{\Omega}}'\cdot\hat{\boldsymbol{\Omega}} - 1) \tag{3.10}$$

where $p'(\hat{\boldsymbol{\Omega}}', \hat{\boldsymbol{\Omega}})$ is the δ-scaled phase function, and f is the fraction scattered in the direction of the forward peak of the phase function, i.e. we approximate the forward peak by an equivalent Dirac δ peak. The factor 2 in the second term arises from the normalisation condition for the phase function (1.15), assuming p' satisfies the same condition.

Integrating (3.8) over the solar radiation δ peak:

$$-\frac{\text{d}S}{\text{d}\tau} = \frac{S}{\mu_0} - \tilde{\omega}f\frac{S}{\mu_0} = \frac{S}{\mu_0}(1 - \tilde{\omega}f) \tag{3.11}$$

---

[3]It should be noted that the true angle at which radiation passes through a layer depends on the layer height, but here an independent scaling was used. It is also affected by refraction, which is omitted as well.

This motivates us to introduce δ-*scaling* $\tau' \equiv \tau(1 - \tilde{\omega}f)$, so that the radiative transfer equation for direct radiation now resembles the Beer's law:

$$\frac{\mathrm{d}S}{\mathrm{d}\tau'} = -\frac{S}{\mu_0} \tag{3.12}$$

3.2.2   Radiative Transfer Equations of Diffuse Radiation

In the δ-two stream approximation, the plane parallel radiative transfer equation (3.2) can be integrated in a closed-form over each hemisphere to get a simplified set of differential equations expressed in terms of upward and downward flux density. Integration over the top hemisphere is:

$$\int_\uparrow \mu \frac{\mathrm{d}I(\hat{\mathbf{\Omega}})}{\mathrm{d}\tau} \mathrm{d}\omega = \int_\uparrow \left[I(\hat{\mathbf{\Omega}}) - (1 - \tilde{\omega})B(\hat{\mathbf{\Omega}}) - \frac{\tilde{\omega}}{4\pi} \int_{4\pi} p(\hat{\mathbf{\Omega}}', \hat{\mathbf{\Omega}})I(\hat{\mathbf{\Omega}}')\mathrm{d}\omega' \right] \mathrm{d}\omega$$

$$\frac{\mathrm{d}F^\uparrow}{\mathrm{d}\tau} = 2F^\uparrow - (1 - \tilde{\omega})2\pi B^\uparrow -$$
$$- \frac{\tilde{\omega}}{4\pi} \left[\int_\uparrow \int_\uparrow p(\hat{\mathbf{\Omega}}', \hat{\mathbf{\Omega}})I^\uparrow \mathrm{d}\omega' \mathrm{d}\omega + \int_\uparrow \int_\downarrow p(\hat{\mathbf{\Omega}}', \hat{\mathbf{\Omega}})I^\downarrow \mathrm{d}\omega' \mathrm{d}\omega + \int_\uparrow \int_\downarrow p(\hat{\mathbf{\Omega}}', \hat{\mathbf{\Omega}})I_{\mathrm{dir}}(\hat{\mathbf{\Omega}}')\mathrm{d}\omega' \mathrm{d}\omega \right] =$$
$$= 2F^\uparrow - (1 - \tilde{\omega})2\pi B^\uparrow - \tilde{\omega} \left[(1 - b)2F^\uparrow + b2F^\downarrow + b_0(1 - f)\frac{S}{\mu_0} \right] \tag{3.13}$$

where we introduced the *backscatter fraction* b and *solar backscatter fraction* b_0:

$$b \equiv \frac{1}{4\pi} \int_\uparrow \int_\downarrow p(\hat{\mathbf{\Omega}}', \hat{\mathbf{\Omega}})I_{\mathrm{diff}}(\hat{\mathbf{\Omega}}')\mathrm{d}\omega' \mathrm{d}\omega \bigg/ \int_\downarrow I_{\mathrm{diff}}(\hat{\mathbf{\Omega}}')\mathrm{d}\omega'$$

$$\equiv \frac{1}{4\pi} \int_\downarrow \int_\uparrow p(\hat{\mathbf{\Omega}}', \hat{\mathbf{\Omega}})I_{\mathrm{diff}}(\hat{\mathbf{\Omega}}')\mathrm{d}\omega' \mathrm{d}\omega \bigg/ \int_\uparrow I_{\mathrm{diff}}(\hat{\mathbf{\Omega}}')\mathrm{d}\omega' \tag{3.14}$$

$$b_0 \equiv \frac{1}{4\pi} \int_\uparrow \int_\downarrow p(\hat{\mathbf{\Omega}}', \hat{\mathbf{\Omega}})I_{\mathrm{dir}}(\hat{\mathbf{\Omega}}')\mathrm{d}\omega' \mathrm{d}\omega \bigg/ \frac{1}{4\pi} \int_{4\pi} \int_\downarrow p'(\hat{\mathbf{\Omega}}', \hat{\mathbf{\Omega}})(1 - f)I_{\mathrm{dir}}(\hat{\mathbf{\Omega}}')\mathrm{d}\omega' \mathrm{d}\omega$$
$$\tag{3.15}$$

which is the fraction of scattered downward radiation scattered upward, and, considering symmetricity of p, it is the same as the fraction of scattered upward radiation scattered downward.

Integration over the bottom hemisphere can be performed analogously to the top hemisphere:

$$\int_\downarrow \mu \frac{\mathrm{d}I(\hat{\mathbf{\Omega}})}{\mathrm{d}\tau}\mathrm{d}\omega = \int_\downarrow \left[I(\hat{\mathbf{\Omega}}) - (1-\tilde{\omega})B(\hat{\mathbf{\Omega}}) - \frac{\tilde{\omega}}{4\pi}\int_{4\pi} p(\hat{\mathbf{\Omega}}',\hat{\mathbf{\Omega}})I(\hat{\mathbf{\Omega}}')\mathrm{d}\omega' \right]\mathrm{d}\omega$$

$$\frac{\mathrm{d}F^\downarrow}{\mathrm{d}\tau} + \frac{\mathrm{d}S}{\mathrm{d}\tau} = 2F^\downarrow + \frac{S}{\mu_0} - (1-\tilde{\omega})2\pi B^\downarrow -$$
$$- \frac{\tilde{\omega}}{4\pi}\left[\int_\downarrow\int_\uparrow p(\hat{\mathbf{\Omega}}',\hat{\mathbf{\Omega}})I^\uparrow \mathrm{d}\omega'\mathrm{d}\omega + \int_\downarrow\int_\downarrow p(\hat{\mathbf{\Omega}}',\hat{\mathbf{\Omega}})I^\downarrow \mathrm{d}\omega'\mathrm{d}\omega + \int_\downarrow\int_\downarrow p(\hat{\mathbf{\Omega}}',\hat{\mathbf{\Omega}})I_{\mathrm{dir}}(\hat{\mathbf{\Omega}}')\mathrm{d}\omega'\mathrm{d}\omega \right] =$$
$$= 2F^\downarrow + \frac{S}{\mu_0} - (1-\tilde{\omega})2\pi B^\downarrow - \tilde{\omega}\left[(1-b)2F^\downarrow + b2F^\uparrow + (1-b_0)(1-f)\frac{S}{\mu_0} + f\frac{S}{\mu_0} \right]$$
$$\text{(3.16)}$$

from which we can subtract the equation for direct radiation (3.11) to get:

$$\frac{\mathrm{d}F^\downarrow}{\mathrm{d}\tau} = 2F^\downarrow - (1-\tilde{\omega})2\pi B^\downarrow - \tilde{\omega}\left[(1-b)2F^\downarrow + b2F^\uparrow + (1-b_0)(1-f)\frac{S}{\mu_0} \right] \quad \text{(3.17)}$$

3.2.3 Delta Scaling

Putting together the derived equations from the previous two sections (3.12), (??), (3.17), the final radiative transfer equations in the δ-two stream approximation are:

$$\frac{\mathrm{d}F^\uparrow}{\mathrm{d}\tau} = 2F^\uparrow - (1-\tilde{\omega})2\pi B^\uparrow - \tilde{\omega}(1-b)2F^\uparrow - \tilde{\omega}b2F^\downarrow - \tilde{\omega}b_0(1-f)\frac{S}{\mu_0} \quad \text{(3.18)}$$

$$-\frac{\mathrm{d}F^\downarrow}{\mathrm{d}\tau} = 2F^\downarrow - (1-\tilde{\omega})2\pi B^\downarrow - \tilde{\omega}(1-b)2F^\downarrow - \tilde{\omega}b2F^\uparrow + \tilde{\omega}(1-b_0)(1-f)\frac{S}{\mu_0}$$
$$\text{(3.19)}$$

$$\frac{\mathrm{d}S}{\mathrm{d}\tau'} = -\frac{S}{\mu_0} \quad \text{(3.20)}$$

We can apply the delta scaling $\tau' = \tau(1-\tilde{\omega}f)$ to the upward and downward flux equations in addition to the direct radiation, and maintain the same structure of the equations by a suitable scaling of $\tilde{\omega}$ and b:

$$\tilde{\omega}' = \tilde{\omega}\left[\frac{1-f}{1-f\tilde{\omega}}\right] \tag{3.21}$$

$$b' = b\left[\frac{1}{1-f}\right] \tag{3.22}$$

$$b_0' = b_0 \tag{3.23}$$

after which the equations for diffuse radiation become:

$$\frac{\mathrm{d}F^\uparrow}{\mathrm{d}\tau'} = 2F^\uparrow - (1-\tilde{\omega}')2\pi B^\uparrow - \tilde{\omega}'(1-b')2F^\uparrow - \tilde{\omega}'b'2F^\downarrow - \tilde{\omega}'b_0'\frac{S}{\mu_0} \tag{3.24}$$

$$-\frac{\mathrm{d}F^\downarrow}{\mathrm{d}\tau'} = 2F^\downarrow - (1-\tilde{\omega}')2\pi B^\downarrow - \tilde{\omega}'(1-b')2F^\downarrow - \tilde{\omega}'b'2F^\uparrow + \tilde{\omega}'(1-b_0')\frac{S}{\mu_0} \tag{3.25}$$

3.2.4 Differential Form of the Radiative Transfer Equation

The equations 3.24, 3.25 and 3.20 can be expressed more concisely using a set of *differential layer coefficients* $\alpha_1, ..., \alpha_4$ (the δ-scaling prime index was dropped for brevity):

$$\frac{\mathrm{d}F^\uparrow}{\mathrm{d}\tau} = \alpha_1 F^\uparrow - \alpha_2 F^\downarrow - \alpha_3\frac{S}{\mu_0} - (\alpha_1 - \alpha_2)\pi B \tag{3.26}$$

$$\frac{\mathrm{d}F^\downarrow}{\mathrm{d}\tau} = \alpha_2 F^\uparrow - \alpha_1 F^\downarrow + \alpha_4\frac{S}{\mu_0} + (\alpha_1 - \alpha_2)\pi B \tag{3.27}$$

$$\frac{\mathrm{d}S}{\mathrm{d}\tau} = -\frac{S}{\mu_0} \tag{3.28}$$

where:

- $\alpha_1 = 2(1 - \tilde{\omega}(1-b))$
- $\alpha_2 = 2b\tilde{\omega}$
- $\alpha_3 = b_0\tilde{\omega}$
- $\alpha_4 = (1 - b_0)\tilde{\omega}$

This system of equations simplifies in both the shortwave and longwave spectrum: in shortwave $B = 0$, in longwave $S = 0$.

3.2.5   Integral Form of the Radiative Transfer Equation for a Homogeneous Layer

The coupled system of linear ordinary differential equations (3.26)–(3.28) can be solved for a homogeneous layer by diagonalisation and subsequent integration. While straightforward, the solution is complicated to perform, and we list only the result here according to Mašek et al. (2014). Also see e.g. Zdunkowski, Trautmann, and Bott (2007), Sec. 6.4 for a worked out solution.

Integrated over a layer from τ_t (top) to τ_b (bottom), the diffuse and direct fluxes have the following linear relationship:

$$\begin{bmatrix} S(\tau_b) \\ F^\downarrow(\tau_b) \\ F^\uparrow(\tau_t) \end{bmatrix} = \begin{bmatrix} a_1 & 0 & 0 \\ a_2 & a_4 & a_5 \\ a_3 & a_5 & a_4 \end{bmatrix} \begin{bmatrix} S(\tau_t) \\ F^\downarrow(\tau_t) \\ F^\uparrow(\tau_b) \end{bmatrix} \tag{3.29}$$

where the *integral layer coefficients* $a_1, ..., a_5$:

$$a_1 = \exp\left(-\frac{\tau}{\mu_0}\right), \quad \tau = \tau_b - \tau_t \tag{3.30}$$

$$a_2 = -a_4\gamma_2 - a_5\gamma_1 a_1 + \gamma_2 a_1 \tag{3.31}$$

$$a_3 = -a_5\gamma_2 - a_4\gamma_1 a_1 + \gamma_1 \tag{3.32}$$

$$a_4 = \frac{E(1 - M^2)}{1 - E^2 M^2} \tag{3.33}$$

$$a_5 = \frac{M(1 - E^2)}{1 - E^2 M^2} \tag{3.34}$$

$$\gamma_1 = \frac{\alpha_3 - \mu_0(\alpha_1\alpha_3 + \alpha_2\alpha_4)}{1 - \epsilon^2\mu_0^2} \tag{3.35}$$

$$\gamma_2 = \frac{-\alpha_4 - \mu_0(\alpha_1\alpha_4 + \alpha_2\alpha_3)}{1 - \epsilon^2\mu_0^2} \tag{3.36}$$

$$E = \exp(-\epsilon\tau), \quad M = \frac{\alpha_2}{\alpha_1 + \epsilon}, \quad \epsilon = \sqrt{\alpha_1^2 - \alpha_2^2} \tag{3.37}$$

The integral layer coefficients can be interpreted as:

- a_1: *direct transmittance*
- a_2: *direct to diffuse transmittance*
- a_3: *direct to diffuse reflectance*
- a_4: *diffuse transmittance*
- a_5: *diffuse reflectance*

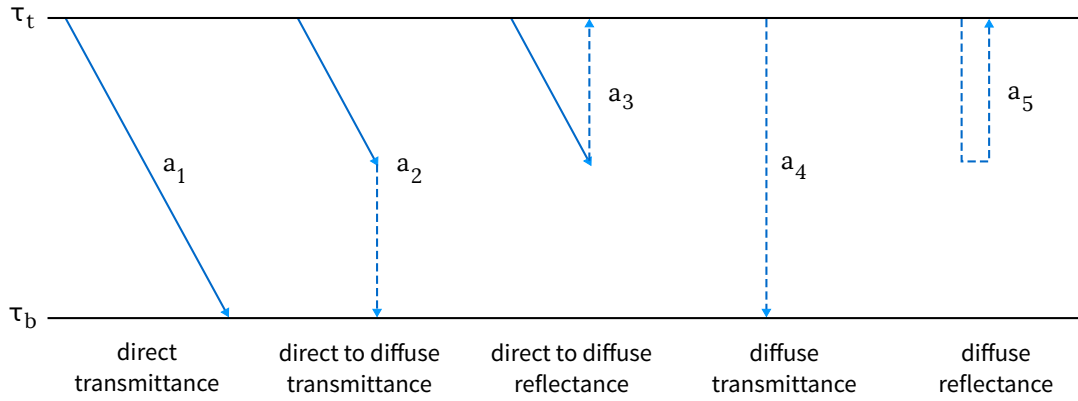The meaning of the coefficients is shown schematically in Figure 3.2.

Figure 3.2: Schematic view of the integral layer coefficients. Full lines indicate direct radiation, dashed lines indicate diffuse radiation passing through an atmospheric layer bounded by optical depths τ_t and τ_b.

3.2.6 Diffusivity Factor

In the simple application of two stream approximation, we assume that diffuse radiation is hemispherically isotropic at all points along the vertical axis z. When integrating vertically over a finite path (a slab of atmosphere), however, we can improve the accuracy if we take into consideration that within the slab radiance may have full directional dependence and preserve hemispheric isotropy on the boundaries only. This allows us to account for the fact that radiation traversing the slab at different angles passes through different path lengths, and thus is subject to different levels of attenuation.

It is possible to introduce a single parameter U, called *diffusivity factor*, into the integral form of the radiative transfer equation to rescale the optical depth, and improve its accuracy significantly.

First, we consider the case of simple Beer's law, i.e. without scattering. In the two stream approximation:

$$\mu\frac{\mathrm{d}I}{\mathrm{d}\tau} = -I \quad / \int_{\downarrow}(...)\mathrm{d}\omega \tag{3.38}$$

$$\frac{\mathrm{d}F_{\downarrow}}{\mathrm{d}\tau} = -2F_{\downarrow} \tag{3.39}$$

$$F_{\downarrow}(\tau) = F_{\downarrow}(0)\exp(-2\tau) \tag{3.40}$$

However, the true $F_{\downarrow}(\tau)$ is:

$$F_{\downarrow}(\tau) = \int_{\downarrow} I(\tau)\hat{\mathbf{n}}\cdot\hat{\mathbf{\Omega}}\,\mathrm{d}\omega = \int_{\downarrow}\int_{0}^{\tau} I(0)\exp(-\tau')\mathrm{d}\tau'\hat{\mathbf{n}}\cdot\hat{\mathbf{\Omega}}\,\mathrm{d}\omega \tag{3.41}$$
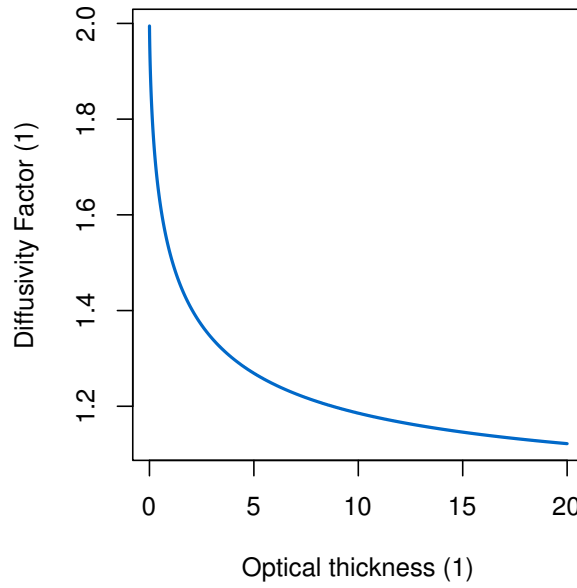
Figure 3.3: Dependence of monochromatic diffusivity factor on optical thickness. Diffusivity factor ranges from 2 for very small optical thickness to 1 for large optical thickness.

If we instead introduce a more flexible form of (3.40) with the diffusivity factor:

$$F_\downarrow(\tau) = F_\downarrow(0) \exp(-U\tau) \tag{3.42}$$

and require that such $F_\downarrow(\tau)$ is the exact flux as in (3.41), we can solve for $U(\tau)$ to get a curve as in Figure 3.3. The values range from 2 for $\tau \ll 1$ (*no scaling* relative to unmodified two stream approximation) to 1 for $\tau \gg 1$.

The situation is more complicated if we consider broadband radiation, where optical saturation modifies the level of attenuation with respect to monochromatic radiation in a path-dependent way. Generally, a single value of U between 1 and 2 is chosen in radiation schemes, such that good practical results are obtained.

3.3 Band Models

Radiatively active gases usually have many more absorption lines than can be integrated over in NWP models in a time-effective manner. A number of statistical approaches to this problem have been invented. One well-established approach is *band models*, whereby line strengths are assumed to have a particular statistical distribution with a limited number of parameters in each band (wavelength interval). For suitably chosen

distributions, the integration over wavelength and a finite path can be done in a closed-form, leading to an expression for band-averaged transmittance as a function of path length and distribution parameters. Traditionally, the band interval has to be small enough, so that radiance (given by the Planck's law) can be assumed constant within the band. Such bands are called *narrow-band*. As discussed later, with some effort this restriction can be lifted, and band models can be applied to much larger *broadband* intervals, such as the entire shortwave or longwave spectrum.

3.3.1   Malkmus Model

One of the most popular narrow-band models is the *Malkmus model*. It is based on the assumption that there is a given number of randomly distributed absorption lines in each band, and their strength has the probability density:

$$p(S) = \frac{1}{S} e^{-S/S_0} \tag{3.43}$$

where $S_0 = \int_0^\infty Sp(S)dS$ is the mean line strength.

Optical depth at wavenumber ν is the sum of contributions of all lines:

$$\tau = ku = \sum_{i=0}^{N} S_i u f(\nu) = \sum_{i=0}^{N} \frac{S_i u \alpha}{\pi[(\nu - \nu_i)^2 + \alpha^2]} \tag{3.44}$$

where $f(\nu)$ is the Voigt line shape, and narrow-band transmittance:

$$\mathcal{T} = \frac{1}{\Delta \nu} \int_{\nu_1}^{\nu_2} e^{-\tau} d\nu = \frac{1}{\Delta \nu} \int_{\nu_1}^{\nu_2} \exp\left(-\sum_{i=0}^{N} \frac{S_i u \alpha}{\pi[(\nu - \nu_i)^2 + \alpha^2]} \right) d\nu \tag{3.45}$$

The above expression is a random variable (because S_i and ν_i are random variables). Therefore, we have to compute the mean to be useful:

$$\bar{\mathcal{T}} = \int_{\mathbf{S}} \int_{\nu} \mathcal{T} p(\nu) p(\mathbf{S}) d\nu d\mathbf{S} \tag{3.46}$$

where $\mathbf{S} = (S_1, ..., S_N)$ and $\nu = (\nu_1, ..., \nu_N)$ are vectors of line strengths and line positions, and p denotes the probability density function. This integration can be performed in a closed-form (see e.g. Zdunkowski, Trautmann, and Bott 2007), leading to the *Malkmus formula* for narrow-band optical thickness:

$$\tau_{\mathrm{M}} = \frac{\pi \alpha}{2\delta} \left(\sqrt{1 + \frac{4\bar{S}u}{\pi \alpha}} - 1 \right) \tag{3.47}$$
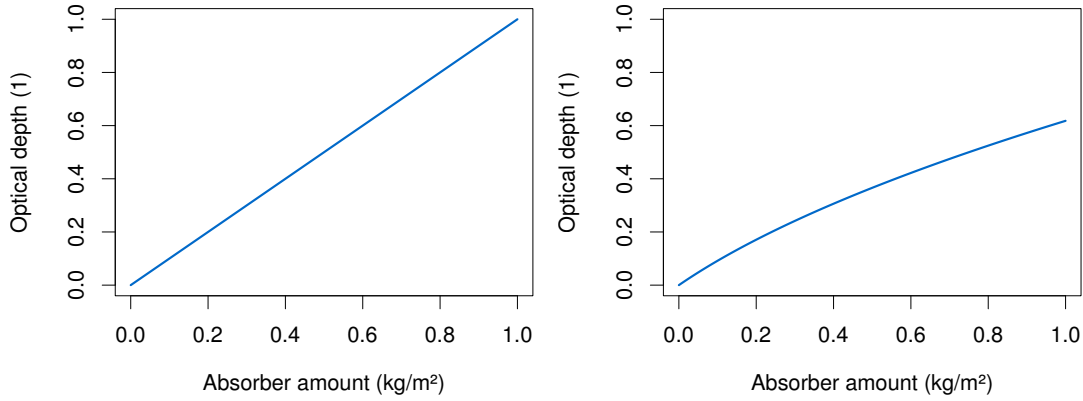
Figure 3.4: Monochromatic and narrow-band optical depth. In the monochromatic case (**left**), the increase in optical depth is linear, whereas in a narrow-band model (**right**) optical saturation causes increase to be progressively more sublinear. Shown is a Malkmus model as in (3.48).

where δ is the average line spacing. This formula can be adapted to the case of non-uniform line width α by comparing two limiting cases of small and large mass paths to the weak and strong line limits derived in Sec. ?. The formula is first written in terms of two parameters a and b:

$$\tau_{\mathrm{M}} = \frac{a}{2b}\left(\sqrt{1 + 4bu} - 1\right) \tag{3.48}$$

By making approximations for $4bu \ll 1$ and $4bu \gg 1$ match the weak and strong line limits, one can show that:

$$a = \sum S_i \tag{3.49}$$

$$b = a^2 / \left(\sum 2\sqrt{S_i\alpha_i}\right)^2 \tag{3.50}$$

3.3.2 Optical Saturation

From the equation for Malkmus model (3.48) we can see that the increase of optical depth with absorber amount u is nonlinear. This phenomenon is sometimes called *optical saturation*, i.e. absorption by an absorption line can contribute to narrow-band optical depth only until substantial fraction of radiation at the wavelength is depleted. After that, the radiation no longer contains certain wavelengths and optical depth increases more slowly. This is in contrast with monochromatic absorption and gray broadband absorption, when optical depth increases linearly with absorber amount at all times (Figure 3.4).

We should note that the asymptotic behaviour of the narrow-band Malkmus model is:

- $\tau \propto u$ for relatively small absorber amount (weak limit)
- $\tau \propto \sqrt{u}$ for relatively large absorber amount (strong limit)

When considering optical depth of larger spectral intervals (where narrow-band approximation no longer applies), we can observe *secondary saturation*, when diminishing rate of optical depth increase is caused by variability of extinction with wavelength such as in Rayleigh scattering, and in cloud absorption and scattering. While this is not an issue to narrow-band model radiation schemes, it has to be taken into account in broadband model radiation schemes *in addition* to optical saturation.

3.4 Adding Method

The *adding method* is a method of finding a solution to fluxes for given optical depths and temperature of layers. The adding method assumes the δ-two stream approximation and layer discretisation.

A relationship between fluxes at the top and bottom interfaces of a layer can be found from the δ-two stream differential equations.

$$\begin{pmatrix} S_k \\ F_k^{\downarrow} \\ F_{k-1}^{\uparrow} \end{pmatrix} = \begin{pmatrix} a_1 & 0 & 0 \\ a_2 & a_3 & a_4 \\ a_5 & a_6 & a_7 \end{pmatrix} \begin{pmatrix} S_{k-1} \\ F_{k-1}^{\downarrow} \\ F_k^{\uparrow} \end{pmatrix} \tag{3.51}$$

The equations for all layers can be consolidated into a system of linear equations:

$$\mathbb{A}\mathbf{F} = \mathbf{S} \tag{3.52}$$

where $\mathbb{A}$ is a matrix of coefficients (layer transmittances and reflectances), $\mathbf{F}$ is a vector of fluxes and $\mathbf{S}$ is a vector of sources. This system can then be solved for $\mathbf{F}$, which is the desired outcome of the adding method.

3.5 Temporal Subsampling

Because the temporal variability of all quantities coming as an input to the RTE is not the same, it is convenient to avoid repeated computation of certain results. E.g., the rate of change of cloud cover is much higher than that of gas concentrations. Therefore, it is possible skip or interpolate gaseous optical thickness. Other intermediate results may also be reused, depending on the actual implementation of the solution.
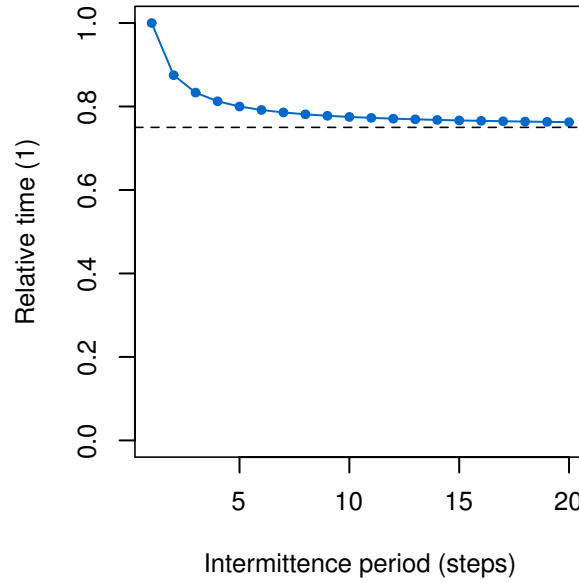
Figure 3.5: Relative model run time with temporal subsampling. The relative run time decreases at a diminishing rate as the intermittency period increases, eventually converging to a constant. In this example, a full step time fraction $q = 0.5$, and intermittent step time fraction $q' = 0.5q$ are assumed.

3.5.1   Diminishing Performance Gain of Temporal Subsampling

Temporal subsampling allows us to reduce the computation time of intermittent steps when approximate results are calculated (e.g. by interpolation), while full steps take an unchanged amount of time (or somewhat greater, depending on implementation details). Radiation schemes constitute a fraction of total run time of an NWP model, typically 20–60 % (?). Therefore, there is a limit on the total time reduction due to performance improvements in the radiation scheme alone. Moreover, as we increase the length of the intermittency period (the number of intermittent steps per the number of full steps), there is a diminishing improvement in total run time, to the point that intermittent steps far outnumber full steps, and the computation time of full steps ceases to matter. The accuracy will continue to decrease, however.

Let us assume that a model time step takes time t_m to compute, and the model initialisation/deinitialisation time is t_0. The total model run time when n steps are computed is then:

$$t(n) = t_0 + t_m n \tag{3.53}$$

If a full step of our module (radiation scheme) takes a fraction q of the model time step

to compute, and an intermittent step takes $q' < q$, and we choose intermittency period of k steps, the total model run time will be:

$$t'_k(n) = t_0 + t_m q \frac{n}{k} + t_m q' \left(n - \frac{n}{k} \right) + t_m (1 - q) n \tag{3.54}$$

i.e. the sum of initialisation time, time of full steps, time of intermittent steps, and the rest of the model. The relative model run time will be:

$$\tau_k = \frac{t'_k(n)}{t(n)} \approx 1 - (q - q') \left(1 - \frac{1}{k} \right) = 1 - q \left(1 - \frac{q'}{q} \right) \left(1 - \frac{1}{k} \right) \tag{3.55}$$

where we neglected the initialisation time ($t_0 \ll t(n)$). Therefore, when $k \to \infty$, $\tau_k \to 1 - (q - q')$, and there is a diminishing gain in performance as k increases.

Figure 3.5 demonstrates τ_k for a particular choice of parameters. We can see that considering improvement in the total model run time is important when deciding the length of the intermittency period, especially considering the detrimental effect intermittency might have the result accuracy.

Chapter 4

Overview of the Radiation Scheme ACRANEB2

ACRANEB2 (J. Geleyn and Hollingsworth 1979; Ritter and J.-F. Geleyn 1992; J. Geleyn, Fournier, et al. 2005; Mašek et al. 2014) is a broadband radiation scheme developed as an alternative to k-distribution radiation schemes. k-distribution schemes, in particular RRTM (E. Mlawer et al. 1997), are currently one of the most popular methods of solving the radiative transfer equation in NWP models, thanks to their superior properties to narrow-band models. Their computation complexity, however, precludes frequent recalculation of fluxes, necessitating either reduced temporal or spatial precision. As a result, changing cloud cover is not resolved with enough accuracy as one might wish. The broadband approach in ACRANEB2 allows for computational intermittency in both shortwave and longwave parts of the spectrum by decoupling quickly changing cloud optical depths from slowly changing gaseous optical depths. This makes calling the radiation scheme at every model time step feasible, responding rapidly to the development of cloud cover.

We can characterise the ACRANEB2 scheme by the choices of methods and approximations:

- Horizontally homogeneous (1D)
- δ-two stream approximation
- Broadband model based (two bands: shortwave and longwave), with modified Malkmus band model transmission approximation
- Curtis-Godson approximation of inhomogeneous path transmission
- Adding method for flux computation to account for multiple scattering in shortwave and longwave spectrum
- Computational intermittency in longwave and shortwave spectrum

ACRANEB2 is currently available as an optional radiation scheme in the NWP model ALADIN of the RC LACE[1] community.

---

[1] Regional Cooperation for Limited Area Modelling in Central Europe (http://www.rclace.eu/).

4.1 Operation Overview

The ACRANEB2 scheme performs calculations independently for every column in the model grid[2]. Vertically, the atmosphere is split into layers, on which the computation is discretised. In the ALADIN model, layers are defined in hybrid *eta coordinates*, transitioning smoothly from σ coordinates near the surface to pressure coordinates in the free atmosphere. Therefore, boundary layers follow the ground, while upper layers follow isobaric surfaces. Apart from an NWP model, ACRANEB2 can be run in isolation inside a single column model. This is useful mostly for diagnostic purposes.

4.1.1 Input and Output

The input to the radiation scheme consists of:

- Pressure profile (definition of layers)
- Temperature profile
- Concentration of gases (water vapour, O_3, CO_2+ composite)
- Cloud fraction and cloud water/ice content
- Aerosol fraction and properties
- Surface temperature, albedo and emissivity Solar constant and the solar zenith angle

The output of the scheme are shortwave and longwave fluxes at layer interfaces, from which the heating rate of layers can be calculated by the NWP model.

4.1.2 Broadband Regions

The ACRANEB2 scheme operates in two spectral regions, matching closely the common distinction between shortwave in longwave spectrum (Sec. 1.1.4):

- Shortwave: 245 nm – 4.642 μm
- Longwave: 4.642 μm – 105.000 μm

In the shortwave spectrum, there is a single source of radiation (the Sun), whereas in the longwave spectrum, the surface and every layer is a source of radiation through thermal emission, but this complexity is somewhat reduced by the fact that scattering of longwave radiation by gases in the atmosphere is weak enough to be neglected, although scattering of longwave radiation by clouds and aerosols still needs to be taken into account.

---

[2]Though in parallel, in order to allow for vectorisation.

4.1.3 General Principle of Operation

The general operation of the scheme can be summarised as follows:

1. Optical thickness and transmittance/reflectance coefficients of layers are calculated. These are due to gases, clouds and aerosols. The resulting layer coefficients are a weighted sum of layer coefficients for the particular processes, weighted by optical thickness (Mašek et al. 2014):

$$\alpha_i = \frac{1}{\tau} \sum_j \alpha_{i,j} \tau_j, \quad \tau = \sum_j \tau_j \tag{4.1}$$

2. Integral layer coefficients $a_1, ..., a_4$ are calculated from $\alpha_1, ..., \alpha_4$.

3. Fluxes are calculated using the adding method, taking the integral layer coefficients as an input.

   Longwave: The adding method is performed in total five times with different choices of 'idealised' optical thickness, i.e. thickness assuming radiation exchanged with the surface, space, or neighbouring layers (resp.).

4.2 Gaseous Transmission

4.2.1 Representation of Gases in ACRANEB2

ACRANEB2 contain representation of all atmospheric gases which contribute significantly to the radiative energy budget in the shortwave and longwave spectrum:

- Water vapour
- O_3
- 'CO2+' (CO_2, CH_4, N_2O, O_2)

where CO_2, CH_4, N_2O and O_2 are treated as a single composite gas ('CO2+'), because they are well-mixed, and their concentration in the atmosphere is relatively constant[3].

---

[3]This is not necessarily true for all conditions, because some of these gases have sources near the surface, e.g. CO_2 is released by vegetation and exhibits both spatial and seasonal variability. Nevertheless, this simplification is justified, because the impact on atmospheric heating rate is small.

4.2.2 Modified Malkmus Model

The radiation scheme depends on the ability to calculate gaseous optical paths between arbitrary layers. Broadband optical paths are approximated by a *modified Malkmus model*. The scheme uses the narrow-band Malkmus band model as its bases, but adding additional parameters in order to account for secondary saturation and Voigt line shape, and increase accuracy over a range of common atmospheric conditions (temperature and pressure).

The modified Malkmus band model is defined as follows (Mašek et al. 2014):

$$\tau_{\mathrm{I}} = \frac{a}{2b}(\sqrt{1 + X(B, Z) + 4bu} - 1)$$

$$\tau_{\mathrm{II}} = \frac{\tau_{\mathrm{crit}}}{\alpha}\left(\left(1 + \frac{\tau_{\mathrm{I}}}{\tau_{\mathrm{crit}}}\right)^{\alpha} - 1\right) \tag{4.2}$$

$$\tau_{\mathrm{III}} = \tau_{\mathrm{II}} \max\left(0, P_{00}(T) + \frac{\tau_{\mathrm{II}}}{\tau_{\mathrm{II}} + D}\sum_{j=0}^{5} P_j(T)(\ln\tau_{\mathrm{II}})^j\right) \tag{4.3}$$

$$\tau_{\mathrm{gas}} = \tau_{\mathrm{III}} \max\left(0, 1 + \frac{Q(p)}{1 + \tau_{\mathrm{III}}}\right) \tag{4.4}$$

where:

- τ_{I} is the narrow-band Malkmus model (3.48) with an additional term $X(B, Z)$, $B = 4bu\alpha_L/\alpha_D$, $Z = \alpha_D/\alpha_L$, in order to account for Doppler broadening of line shape (J. Geleyn, Fournier, et al. 2005).

- τ_{II} is an expression to modify the asymptotic power behaviour of τ_{I} with respect to u to $u^{\alpha/2}$.

- τ_{III} and τ_{gas} are secondary corrective fits, in order to obtain greater accuracy in heating rates. P and Q are second order polynomials in temperature and pressure (resp.).

The final formula τ_{gas} involves 33 parameters, which need to be fitted for a broad range of atmospheric conditions to a reference model. The reference model is a narrow-band model with 408 bands. Reference broadband optical paths are calculated for a set of (u, p, T) combinations by a weighted average of the narrow-band optical paths, weighted by the spectral composition of the incoming solar flux.

4.3 Solving the RTE

The solution for broadband flux densities at layer interfaces is found by multiple passes of the adding method outlined in the previous chapter. The adding method allows for only single absorption and scattering coefficient to be specified per layer. While this is sufficient for monochromatic calculations when the absorption and scattering co-efficients are independent from the flux density, in broadband calculations the power distribution of the flux needs to be taken into account. This is however not possible when fluxes combine contributions from multiple sources, with radiation having traversed different paths through the atmosphere.

One solution to the problem would be to carry out the adding method for every radiation source independently, and summing up the resulting fluxes (which can be done thank to linearity of the RTE). The power distribution of a broadband flux at a layer interface can then be known, because it is determined by the power distribution of the emitting source and the extinction along the path between the source and the layer. To be precise, the path traversed by radiation between the source and the layer is not known with full accuracy, because apart from the direct path, a fraction of the radiation can be scattered multiple times, taking a longer path before arriving at the layer.

While the method outlined above is feasible and relatively accurate, it is too computationally demanding to be performed at every time step, because the adding method would have to be repeated for each layer in the thermal spectrum (every layer is a source of radiation). The number of passes can be reduced when we consider the net exchange rate formulation:

i.e. when we compute the flux divergence R_k by the adding method, it is equal to the sum of CTS, EWS and EBL terms. For a suitable choice of sources,

Chapter 5

Shortwave Intermittency in ACRANEB2

As the atmospheric gaseous composition and temperature and pressure profile do not change as quickly as the cloud cover, we can speed up radiative computations by calculating gaseous optical thickness of layers less frequently than the rest of the fields, while maintaining rapid response to changing cloud cover. In other words, we can introduce a *shortwave intermittency* period longer than the model time step during which the gaseous optical thickness is reused.

In the thermal part of the spectrum, we can achieve this by simply maintaining constant gaseous optical thickness during the intermittency period. In the shortwave spectrum, however, the situation is complicated by the fact that optical thickness depends on the solar zenith angle. It is therefore necessary to devise a method of accounting for this change without the need to do a full (computationally expensive) recalculation of optical thickness.

This chapter discusses the proposal, implementation and evaluation of shortwave intermittency in the context of a single column model and the NWP model ALADIN.

5.1 Theoretical Considerations

5.1.1 Monochromatic Light

Let us first consider the simple case of monochromatic radiation passing through a homogeneous atmospheric layer. Direct radiation passing at cosine of the zenith angle μ_0 is attenuated exponentially by the Beer's law:

$$I(z) = I(z_0) \exp\left(-\frac{1}{\mu_0} k_e \Delta u\right) \tag{5.1}$$

where k_e is the mass extinction coefficient and Δu is the mass of the absorber per unit area. Here, $(1/\mu_0)k_e\Delta u$ is the *optical path* through the layer.

In addition to *optical path*, we use the concept of *optical thickness*. The *optical thickness* of a layer is commonly defined as the optical path through the layer in the vertical direction ($\mu_0 = 1$), but we note that this is the same as normalising the actual optical path by μ_0:

$$\tau := \tau(z_1, z_2; \mu_0 = 1) = k\Delta u = \mu_0 \left(\frac{1}{\mu_0} k\Delta u \right) = \mu_0\tau(z_1, z_2; \mu_0) \qquad (5.2)$$

where $\tau(z_1, z_2; \mu_0)$ denotes optical path for radiation passing at cosine of the zenith angle μ_0. We use the same symbol τ for optical thickness and optical depth, but stating its meaning explicitly where needed. In the monochromatic case, both definitions are equivalent, but the latter generalises better to the broadband radiation treatment, where the Beer's law no longer holds. We will therefore use this latter definition:

$$\tau := \mu_0\tau(z_1, z_2; \mu_0) \qquad (5.3)$$

5.1.2   Downward and Upward Broadband Optical Thickness

In a broadband radiative transfer scheme, it is necessary to distinguish downward and upward optical thickness of a layer. This is because the optical thickness depends not only on the properties of the layer (as in monochromatic case), but also the spectral composition of the radiation entering the layer and the length of the path through the layer, which determines the amount of spectral saturation.

The downward shortwave optical thickness is calculated for parallel radiation coming directly from the Sun at a zenith angle θ and is equal to the optical path through the layer normalised by cosine of the zenith angle (which is proportional to the length of the path).

The upward shortwave optical thickness, on the contrary, is calculated for diffuse radiation reflected from the surface, which does not have any associated direction in the δ-two stream approximation. In this case, the dependence on the zenith angle is only through its influence on the spectrum of the incoming radiation, which has passed through the atmosphere as parallel radiation at the given zenith angle.

The geometry of the downward case is depicted in Fig. 5.1.

5.1.3   Modified Cosine of the Zenith Angle

The actual angle at which radiation passes through an atmospheric layer is not the same as the zenith angle. This is due to the sphericity of the atmosphere, and is particularly true for high zenith angles ($\mu_0 \to 0$).

In order to transparently account for this effect, the ACRANEB2 scheme uses a modified cosine of the zenith angle in place of μ (Mašek et al. 2014):

$$\mu_0' = \frac{1}{\left(\left(\frac{a}{H}\mu_0\right)^2 + 2\frac{a}{H} + 1\right)^{1/2} - \frac{a}{H}\mu_0} \tag{5.4}$$

where a is the radius of the Earth, and H is the approximate height of the atmosphere. The ratio H/a was chosen to be a constant of 0.001324, for which $\mu_0'(\mu_0 = 0) = 38.88$[1]. This has an additional benefit of preventing $1/\mu_0$ growing to infinity as $\mu_0 \to 0$ in numerical calculations.

The modified cosine of the zenith angle is the natural coordinate for studying the change of optical thickness with the position of the Sun in the sky.

5.2   Analysis in a Single Column Model

In order to empirically investigate dependence of broadband gaseous optical thickness on the zenith angle, we used a single column model to calculate optical thickness for varying values of the modified cosine of the zenith angle. We analysed the result of multiple runs of the acra2 SCM model over a range of μ_0 values from the interval $[0, 1]$ to simulate shortwave gaseous optical thickness of layers[2].

5.2.1   Dependence of Optical Thickness on the Zenith Angle

The plot in Fig. 5.2 shows the result for a clear sky atmosphere with 87 layers in standard and log-log coordinates. The dependence is plotted as a function of the modified cosine of the zenith angle (see above). As you can see from the logarithmic plot, the dependence is close to a power function (i.e. is linear in the logarithmic coordinates). This suggest that a linear interpolation between extreme values of the zenith angle in an intermittency period could yield accurate enough results. Similar relationship was observed in cloudy atmosphere and a number of additional cases.

5.2.2   Linear Interpolation of Optical Thickness

As justified by the empirical analysis of optical thickness dependence on the zenith angle, we performed an experiment with the single column model where the log optical

---

[1] It should be noted that the true angle at which radiation passes through a layer depends on the layer height, but here an independent scaling was used. It is also affected by refraction, which is omitted as well.

[2] The full analysis is available at https://github.com/peterkuma/shortwave-intermittency.
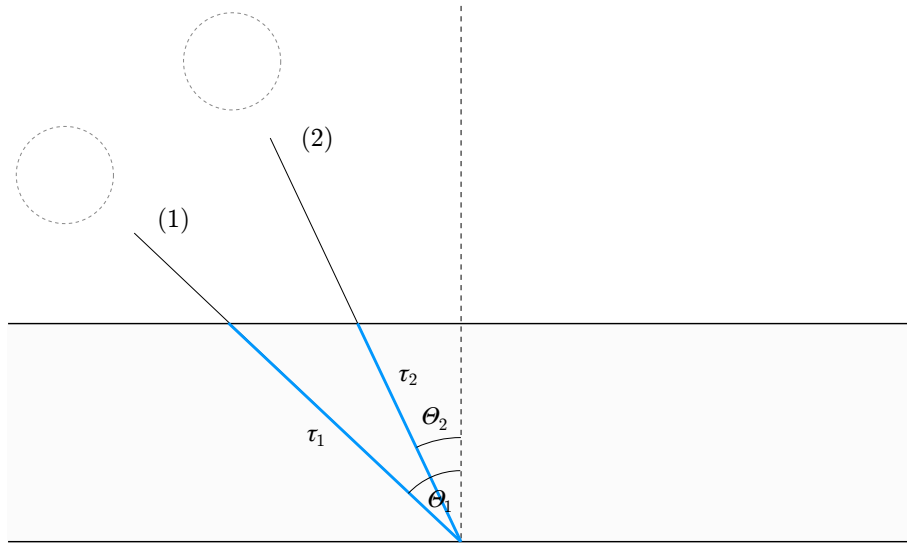
Figure 5.1: Geometry of the shortwave intermittency problem (downward). (1) At the beginning of the intermittency period, solar radiation passes through a plane-parallel atmospheric layer at zenith angle θ_1. (2) As the Sun rises to zenith angle θ_2, the broadband optical thickness (as per our definition) of the layer changes from τ_1 to τ_2. Note that $\tau_2 > \tau_1$, as the broadband optical thickness equals to optical path normalised by $\mu = cos(\theta)$, which is proportional to the length of the path.

thicknesses were linearly interpolated with respect to log of the modified cosine of the zenith angle. The Fig. 5.3 shows the result for a clear-sky atmosphere, and a choice of shortwave intermittency interval of $\Delta\theta = 15°$ (1 h on the equator on equinox). The heating rates were compared to the reference (non-interpolated) case. The difference in heating rates was the most significant for high zenith angles (low $\cos(\mu)$), when the change in the zenith angle corresponds to a large change in the cosine of the zenith angle. The difference was within 0.1 K/day (5 %) for all but the top layers, which is an acceptable loss of accuracy compared to the rest of the broadband radiative scheme.

5.2.3 More Cases

We performed the same analysis as above on multiple other cases: a *cloudy atmosphere* with the same temperature and composition profiles, *tropical*, *midlatitude summer* and *winter* atmospheres, and *subarctic summer* and *winter* atmospheres[3]. The cloudy atmosphere did not differ significantly from the clear sky case. The tropical, midlatitude and subarctic cases had error of the heating rate within 0.5 K/day.

---

[3]Plots of all studied cases can be found in the Additional Materials (see the end of this report).
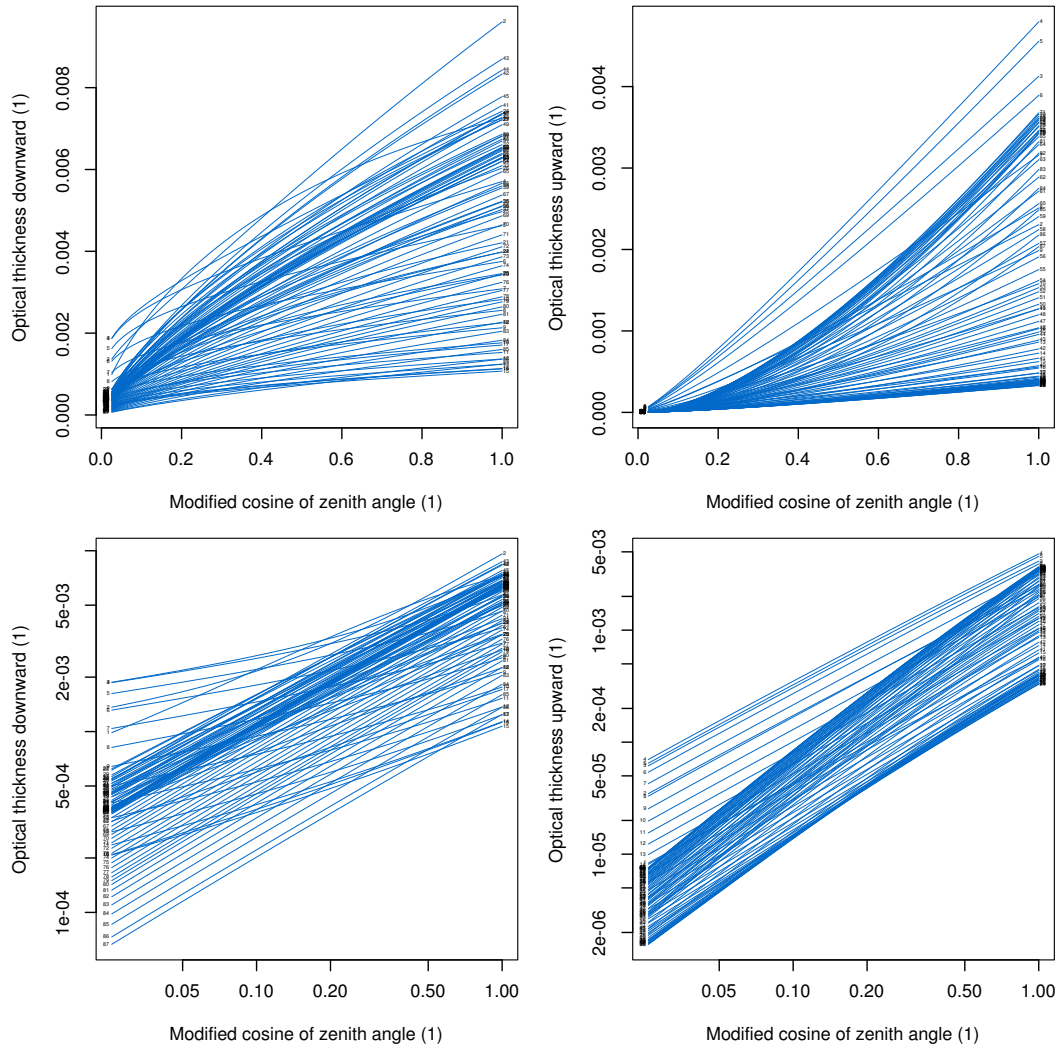
Figure 5.2: Optical thickness of layers as a function of the modified cosine of the zenith angle. Downward optical thickness in ordinary (**top-left**) and log-log coordinates (**bottom-left**), and upward optical thickness in ordinary (**top-right**) and log-log coordinates (**bottom-right**). Lines are labelled with layer numbers. Note that the relationship is almost linear in the log-log coordinates.
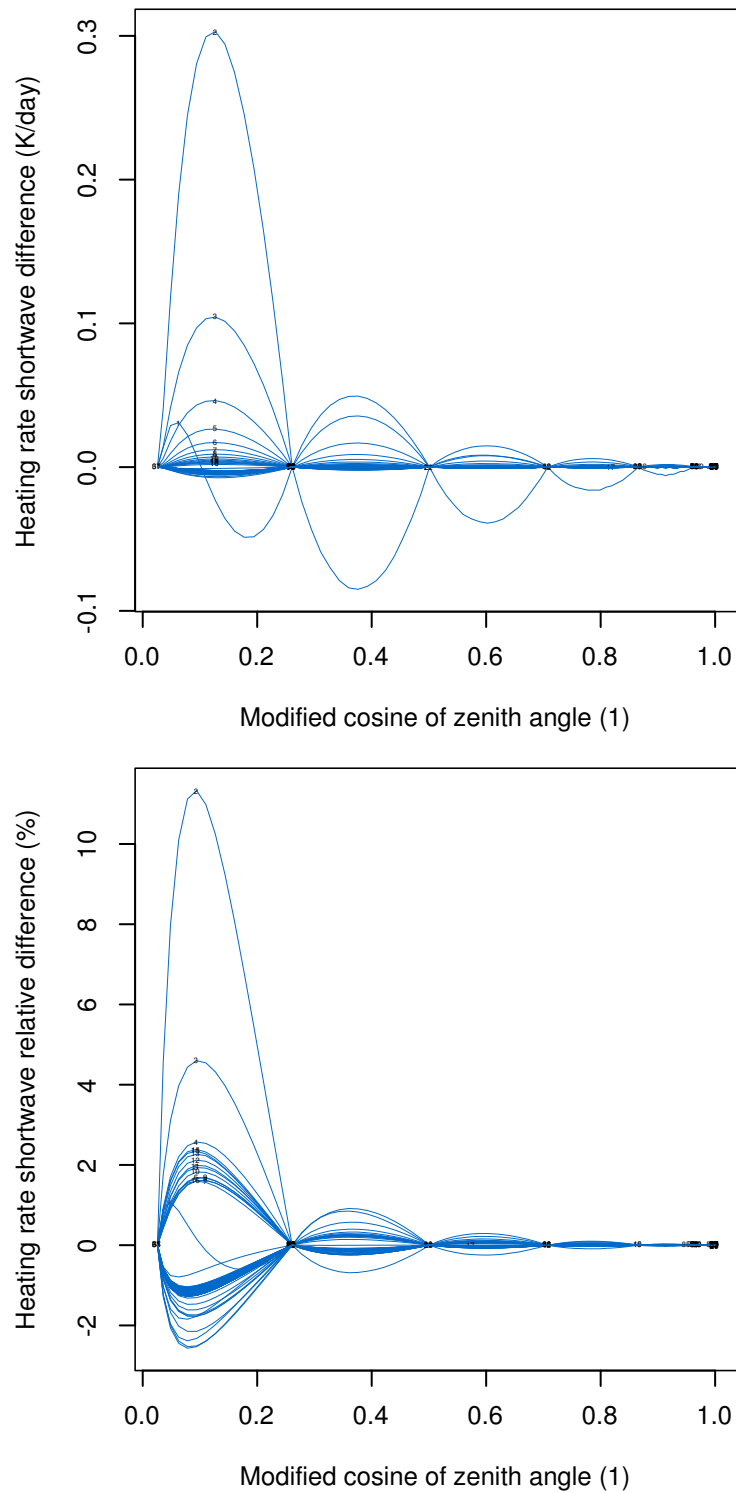
Figure 5.3: Heating rate difference between the reference and linearly interpolated optical thicknesses at 15° steps of the zenith angle. Plots show absolute difference in heating rate (**top**), and relative difference in heating rate in per cent (**bottom**).

5.3   Shortwave Intermittency Implementation in a 3D Model

The results from the Single Column Model support the application of shortwave intermittency in a 3-dimensional NWP model. This was implemented in the ACRANEB2 scheme in the ALADIN[4] model.

In the 3D model, the radiative transfer scheme calculates radiative transfer independently for each grid point of the model domain.

5.3.1   Overview of the Implementation

At the beginning of an intermittency period (*full* radiative time step):

1. Calculate the minimum and maximum values of the zenith angle attained at any time step during the intermittency period. Store the zenith angles (the extreme values as well as the values at all time steps) in global arrays (preserved across time steps).

2. Calculate shortwave optical thickness as usual for the two extreme values the zenith angle. Store (the logarithm of) the optical thicknesses in global arrays.

At every time step *within* the intermittency period (*partial* radiative time step):

1. Retrieve current zenith angle from the global array (ignoring the zenith angle supplied by the model), and continue all computations with this zenith angle.

2. Calculate optical thicknesses by interpolating between the extreme optical thicknesses as stored in the global arrays.

5.3.2   Technical Considerations

There were a number of additional technical considerations which needed to be taken into account when implementing shortwave intermittency in a 3D model:

1. **Solar declination.** Solar declination varies during the intermittency period. In our case, the model does no provide the scheme with solar declination for the subsequent time steps, nor a straightforward way of calculating it[5]. In order to simplify implementation, solar declination within intermittency period is kept constant. This is justified since the length of the intermittency period is not expected to be chosen long enough for the variation of solar declination to be important.

---

[4]ALADIN cycle 38.

[5]Without copying a significant amount of code.

2. **Storage requirements.** Shortwave intermittency requires us to store fields of downward and upward optical thickness at two extreme values of the zenith angle. This results in four 3D global fields of optical thickness and a number of 2D global fields of zenith angles to be kept in the main memory between time steps.

3. **Day/night segmentation.** The ACRANEB2 scheme performs calculations on blocks of grid points in a vectorisable form[6]. The shortwave computations are only performed on segments of grid points where the Sun is in the sky. This selection has to be extended with grid points where the zenith angle is positive at any time during the intermittency period.

4. **Modularisation.** The shortwave intermittency implementation required more modularisation in terms of decoupling the shortwave and longwave computations of optical thickness.

5.4   Analysis Description

In order to evaluate accuracy and performance of the implementation of shortwave intermittency, we performed a number of simulations (experiments) with the ALADIN limited-area NWP model and analysed the results for accuracy and performance.

The simulations were performed on a domain covering Central Europe with coupling to the ARPEGE global model. The horizontal mesh size was 4.7 km with 87 vertical layers and time step of 3 min. Values for offline analysis were sampled from a limited number of points chosen evenly from the whole domain (Figure 5.4). A 24-h summer day convective situation starting at 0:00 UTC, 29 May 2009 was chosen for the analysis.

For the purpose of gathering data from the selected points during model runs, tools called nc_dump[7] and dump2h5[8] for the ALADIN model were developed. These made it possible to export fields into NetCDF/HDF5 files, which were subsequently analysed using a set of short programs made in the statistical programming language R[9].

The runs were made on 8 CPUs of the NEC SX-9 supercomputer (100 GFLOPS per CPU), and performance was measured as the CPU time in an exclusive (benchmark) mode of the machine, in order to avoid interference with other concurrent tasks (which would be substantial). The SX-9 processors rely heavily on code vectorisation, and as such may be less representative of other more common architectures. Multithreading in the ALADIN model is implemented using OpenMP, distributing computation on blocks of grid points to the threads.

---

[6]In the sense of performing an operation on a sequence of values simultaneously by a single processor (on processors which support such a feature).

[7]https://github.com/peterkuma/nc_dump

[8]https://github.com/peterkuma/dump2h5

[9]The full analysis is available at https://github.com/peterkuma/
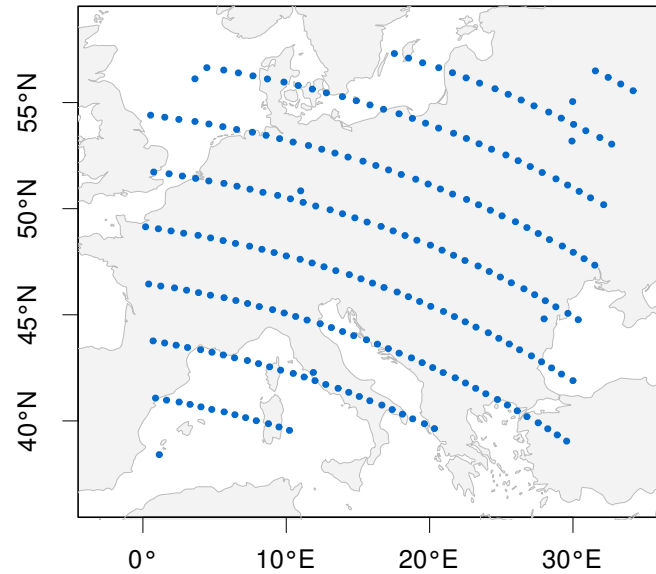
Figure 5.4: Points on the model domain sampled for offline analysis. Data from the points shown were saved during model runs for later (offline) analysis at every time step of the simulation.

5.4.1 Experiments

The following experiments were performed:

1. **Shortwave Intermittency Base**

   Base configuration for shortwave intermittency evaluation:

   - Shortwave gaseous optical thickness computed at every time step.
   - Longwave gaseous optical thickness computed once per 1 h.
   - Calibration of longwave NER weights computed once per 3 h.

2. **Shortwave Intermittency 6-min, 15-min, 30-min, 1-h, 90-min, 2-h**

   Shortwave intermittency enabled with 6-min, 15-min, 30-min, 1-h, 90-min, 2-h intermittency period (resp.):

   - Based on *Shortwave Intermittency Base*.
   - Shortwave gaseous optical thickness computed once per 6 min, 15 min, 30 min, 1 h, 90 min, 2 h (resp).

5.5   Results

5.5.1   Accuracy

In order to determine how shortwave intermittency affects accuracy, we looked at the global bias in heating rate, as well as the local error and its statistical distribution. The shortwave intermittency runs were compared to the base configuration with no shortwave intermittency. The impact on shortwave heating rates and longwave heating rates can be seen in Figure 5.5 and Figure 5.6, resp. The impact on bias was negligible (< 0.2 K/day) in both shortwave and longwave heating rates.

It should be noted that in the time series plot, the time axis is in UTC, therefore domain points are not synchronised with respect to local solar time.

From the shortwave heating rate error time series plot, it is clear that the magnitude of error is the greatest during the day (up to 0.4 K/day with 2-h shortwave intermittency), whereas during the night the error is zero. At the 'full' steps when shortwave gaseous optical depths are calculated, the error drops markedly, giving rise to a tooth-like pattern, but a non-reducible error accumulates with time as the run diverges from the reference run.

Shortwave intermittency has an impact on the longwave heating rates, leading to error of about 0.6 K/day in the second half of the simulation, i.e. greater than in shortwave heating rates. This is likely due the strong sensitivity of longwave fluxes on the temperature profile.

5.5.2   Performance

The total model run time of shortwave intermittency experiments is displayed in Figure 5.7. The time reduction was up to about 5 % with the longest shortwave intermittency period (2 h). There is a diminishing gain in performance with longer intermittency periods, as discussed theoretically in Section 3.5. The 6-min shortwave intermittency run was longer than the base run, which is expected as in every 'full' step of shortwave intermittency gaseous optical thickness is calculated twice (for the start and the end of the forthcoming intermittency period), and the implementation only introduces overhead compared to the base configuration.

Note: It has to be noted that the performance analysis had to be performed with day/night segmentation disabled, as it causes the model run time to be non-monotonic with the length of the shortwave intermittency interval. With day/night segmentation enabled, time reduction scales up to 96 % in the 2-h shortwave intermittency case, whereas in the results presented, the reduction is up to 94 % (i.e. more pronounced). We believe that this choice is justified by the improved clarity of interpretation of the results.

Figure 5.8 compares performance and accuracy of the model runs. As such, it is important in deciding the optimal choice of shortwave intermittency period. The exact choice depends on the presence of other performance tuning options in the whole model configuration, as an option with the least error incurred per reduction in time should be chosen. Therefore, depending on the circumstances it may be viable to increase the shortwave intermittency period even over 1 h, although after this point the error starts to grow more rapidly with respect to any time reduction. Moreover, there is a hard bound on the time saved by shortwave intermittency – when all but the first time step are 'intermittent'. From these results, we can expect it to be about 6–7 %. Users of the radiation scheme are therefore advised to use this chart as a guide in deciding the optimum configuration in their particular situation.

We should remark that the error observed in the runs was not normally distributed. Rather, many local errors were clustered around zero, decreasing gradually in number towards the 95-th percentiles, with the rest distributed in heavy-tails. Therefore, we chose the 90 % confidence intervals and the mean absolute error (MAE) to present our results instead of the more traditional root-mean-square error (RMSE), which would place very strong emphasis on the outliers and could be misleading due to the expectation of normal distribution. However, we realise that the presence of outliers is not a desirable property, but a more complex analysis would need to be performed in order to determine what their source is and whether they can be eliminated.
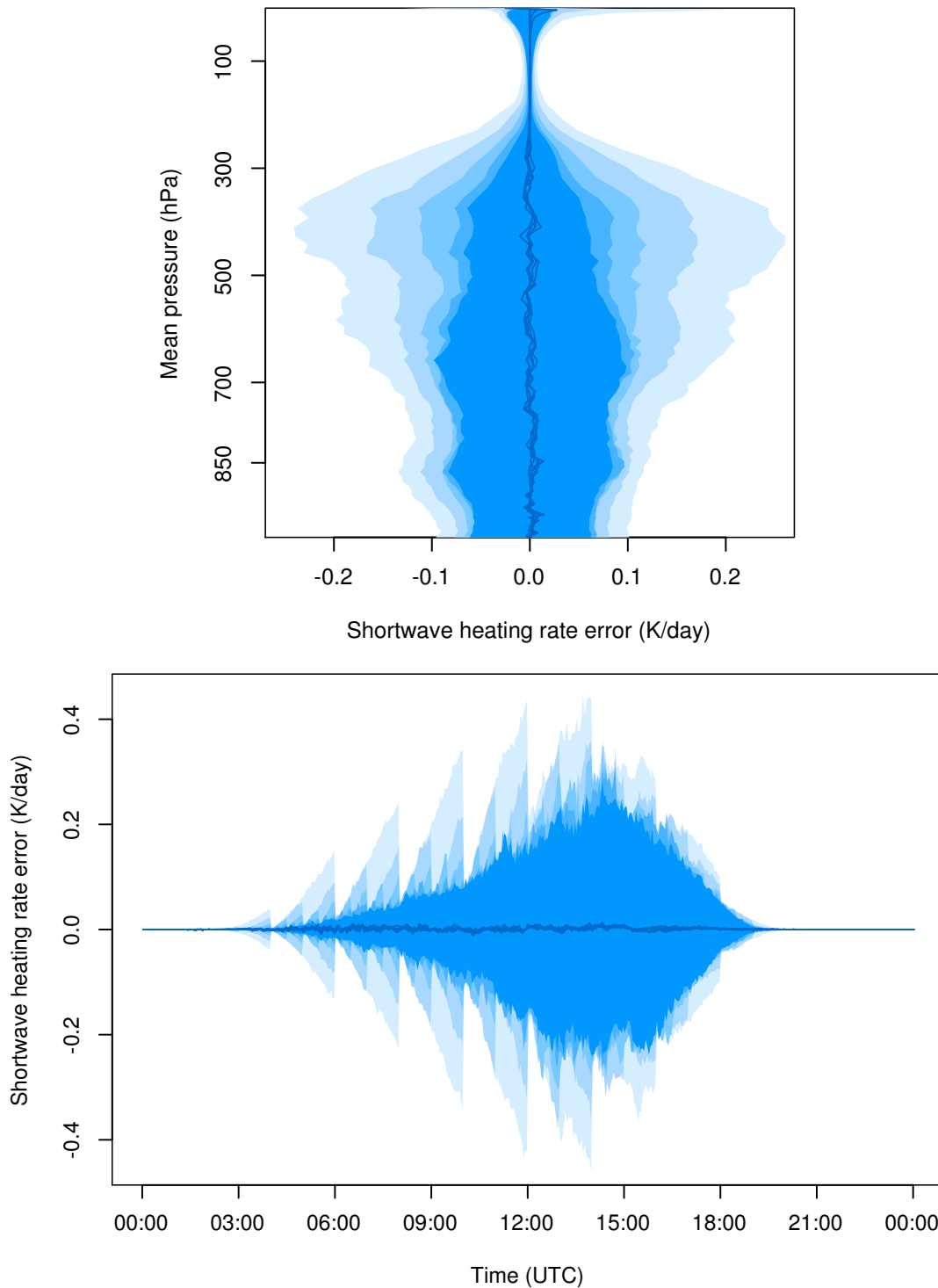
Figure 5.5: Impact of shortwave intermittency on shortwave heating rate error. Shown is a global bias (**top**) and time series (**bottom**) of heating rate and 90 % confidence bands of 24-h model runs with 6 min, 15 min, 1 h, 1.5 h and 2 h shortwave intermittency compared to no shortwave intermittency (bands in progressively lighter shades, resp.). In the time series plot heating rate error is weighted by pressure thickness of layers (by resampling). The situation is a convective summer day of 29 May 2009 over Central Europe.
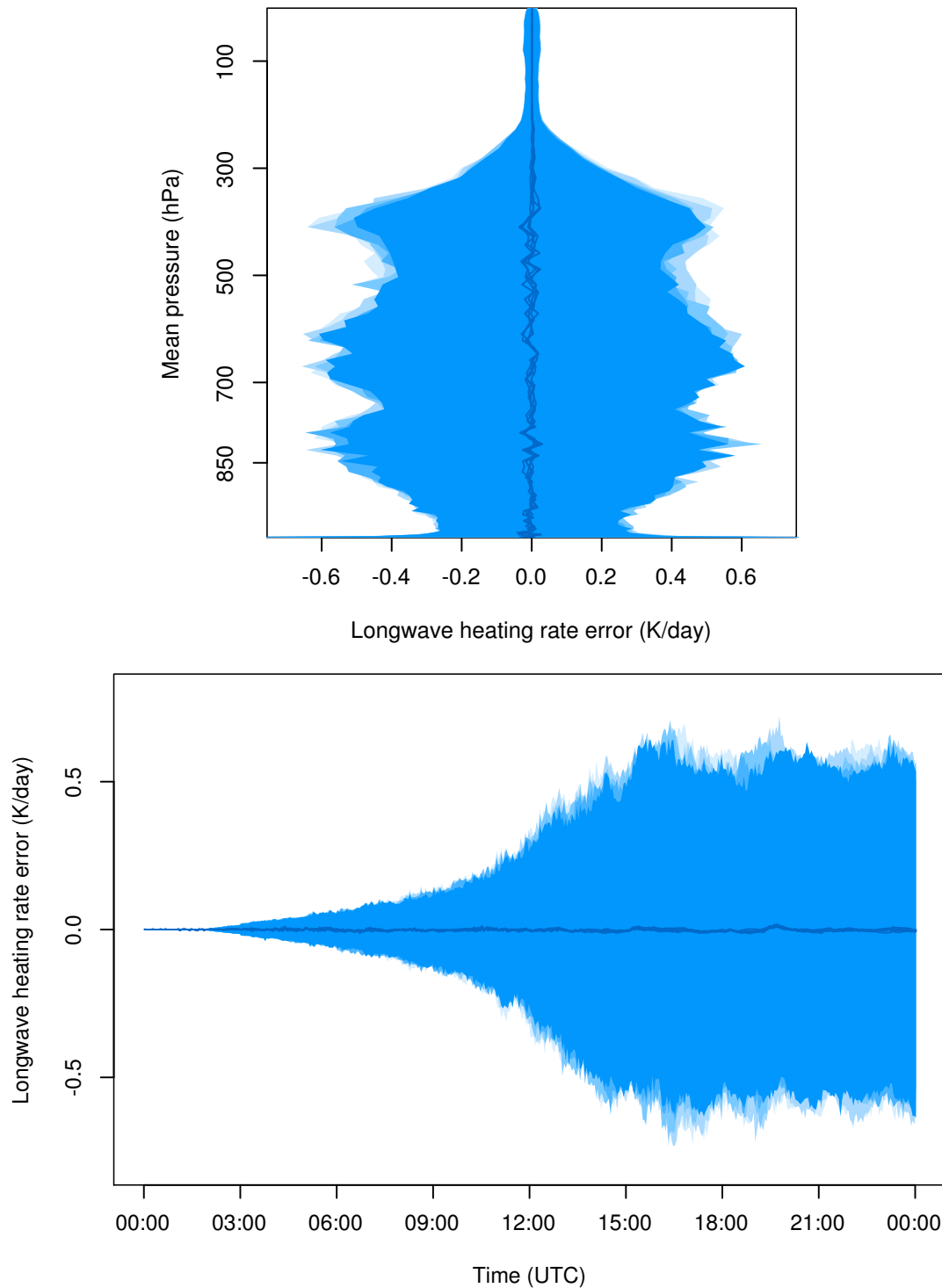
Figure 5.6: Impact of shortwave intermittency on longwave heating rate error. Shown is a global bias (**top**) and time series (**bottom**) of heating rate and 90 % confidence bands of 24-h model runs with 6-min, 15-min, 30-min, 1-h, 1.5-h and 2-h shortwave intermittency compared to no shortwave intermittency (bands in progressively lighter shades, resp.). In the time series plot heating rate error is weighted by pressure thickness of layers (by resampling). The situation is a convective summer day of 29 May 2009 over Central Europe.
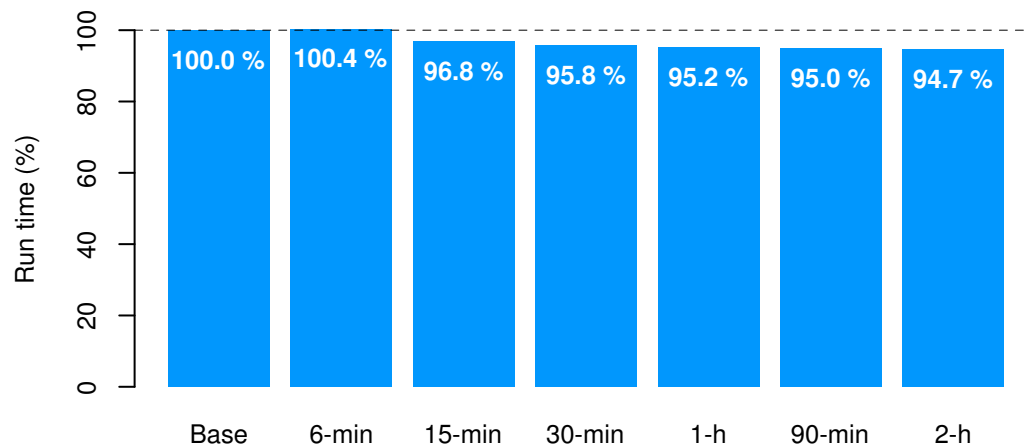
Figure 5.7: Shortwave intermittency performance. Total model run time of shortwave intermittency runs relative to no shortwave intermittency ('Base'). Run time was measured as CPU time in a benchmark (exclusive) mode on 8 CPUs of NEC SX-9 (100 GFLOP per CPU).
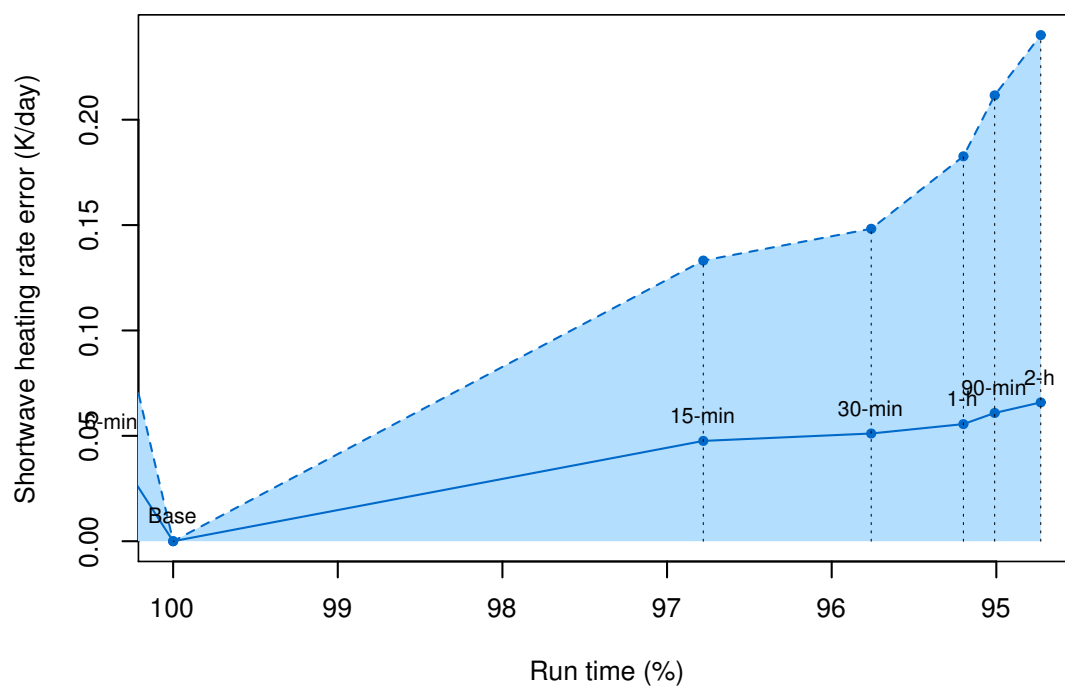

Figure 5.8: Shortwave intermittency performance vs. accuracy. Total model run time and mean absolute heating rate error (**solid line**) of shortwave intermittency runs, relative to no shortwave intermittency. Shown is the 95-% upper bound of the absolute heating rate error across domain sample points and time steps (**dashed line**). Heating rate error is weighted by pressure thickness of layers. Run time was measured as CPU time in a benchmark (exclusive) mode on 8 CPUs of NEC SX-9 (100 GFLOP per CPU).

Conclusion

Appendix A

ACRANEB2 Configuration Parameters

This appendix documents some of the configuration parameters used in the ACRANEB2 radiation scheme, esp. those relevant to computational intermittency. The parameters are set as variables in a Fortran namelist supplied to the SCM (single column model) or the NWP model ALADIN. More configuration parameters are documented briefly in `Arp/module/yomphy.F90` in the ALADIN source code.

A.1   Intermittency Parameters

A.1.1   NSORAYFR

```
NSORAYFR=<n>
NSORAYFR=-<h>
```

Shortwave (solar) intermittency interval length. Shortwave gaseous optical thickness is calculated every `<n>` steps, resp. every `<h>` hours.

A.1.2   NRAUTOEV

```
NRAUTOEV=<n>
```

Intermittency interval of calculation of NER 'bracketing' weights in the thermal (long-wave) computation. Weights are calculated every `<n>` full radiation steps, or disabled when `<n>` = 0.

A.1.3   LRAYPL

```
LRAYPL=.T.|.F.
```

Turn on or off day/night slicing of grid blocks. If enabled, shortwave computation is restricted to 'day' grid cells, possibly improving performance.

A.1.4 NTHRAYFR

```
NTHRAYFR=<n>
NTHRAYFR=-<h>
```

Longwave (thermal) intermittency interval length. Longwave gaseous optical thickness is calculated every <n> steps, resp. every <h> hours.

Appendix B

Comparison of Intermittency in ACRANEB2 and FMR

In this appendix we present the results of an analysis comparing intermittency in ACRANEB2 and FMR (Fouquart and Bonnel 1980)[1]. Both radiation schemes are available in the limited-area model ALADIN. Therefore, it was possible to compare longwave and shortwave intermittency in ACRANEB2 to full intermittency in FMR, relative to their respective base configurations with no intermittency. This analysis is limited in scope, as we compared only 1-h longwave and shortwave intermittency in ACRANEB2 to 1-h full intermittency in FMR (fluxes assumed constant within the intermittency period). The method of analysis and situation were identical to the one described in Section 5.4. The purpose of this analysis was to contrast the effect of full intermittency and partial intermittency of the same length on heating rate error.

In total 4 experiments were performed:

1. **Intermittency Base**

   Base configuration of ACRANEB2 with longwave and shortwave intermittency disabled.

2. **Intermittency 1 h**

   ACRANEB2 with longwave and shortwave intermittency enabled with 1-h period.

   - Based on Intermittency Base.
   - Longwave and shortwave gaseous transmissivities computed once per 1 h.
   - Longwave 'bracketing' weights computed once per 3 h.

---

[1]The results of this analysis are presented in appendix, because the limited scope would not warrant a chapter on its own. Moreover, a proper discussion would require the introduction of a number of concepts related to longwave intermittency in ACRANEB2, for which documentation is yet to be available via a dedicated article (in preparation at the time of writing).

3. **Intermittency FMR Base**

   Base configuration of FMR with intermittency disabled.

4. **Intermittency FMR 1 h**

   FMR with full intermittency enabled with 1-h period.

   - Based on Intermittency FMR Base.
   - Fluxes computed once per 1 h.

Figure B.1 and Figure B.2 show the results obtained from these experiments. It is clear that the longwave and shortwave intermittency implementation in ACRANEB2 is superior to full intermittency in FMR with the same choice of intermittency period. A notable exception are layers below 750 hPa in the longwave spectrum, which would warrant an additional investigation. It should be stressed, however, that this is not a fair comparison in terms of performance, as in this case the 1-h intermittency run of ACRANEB2 takes about 20 % longer than FMR.
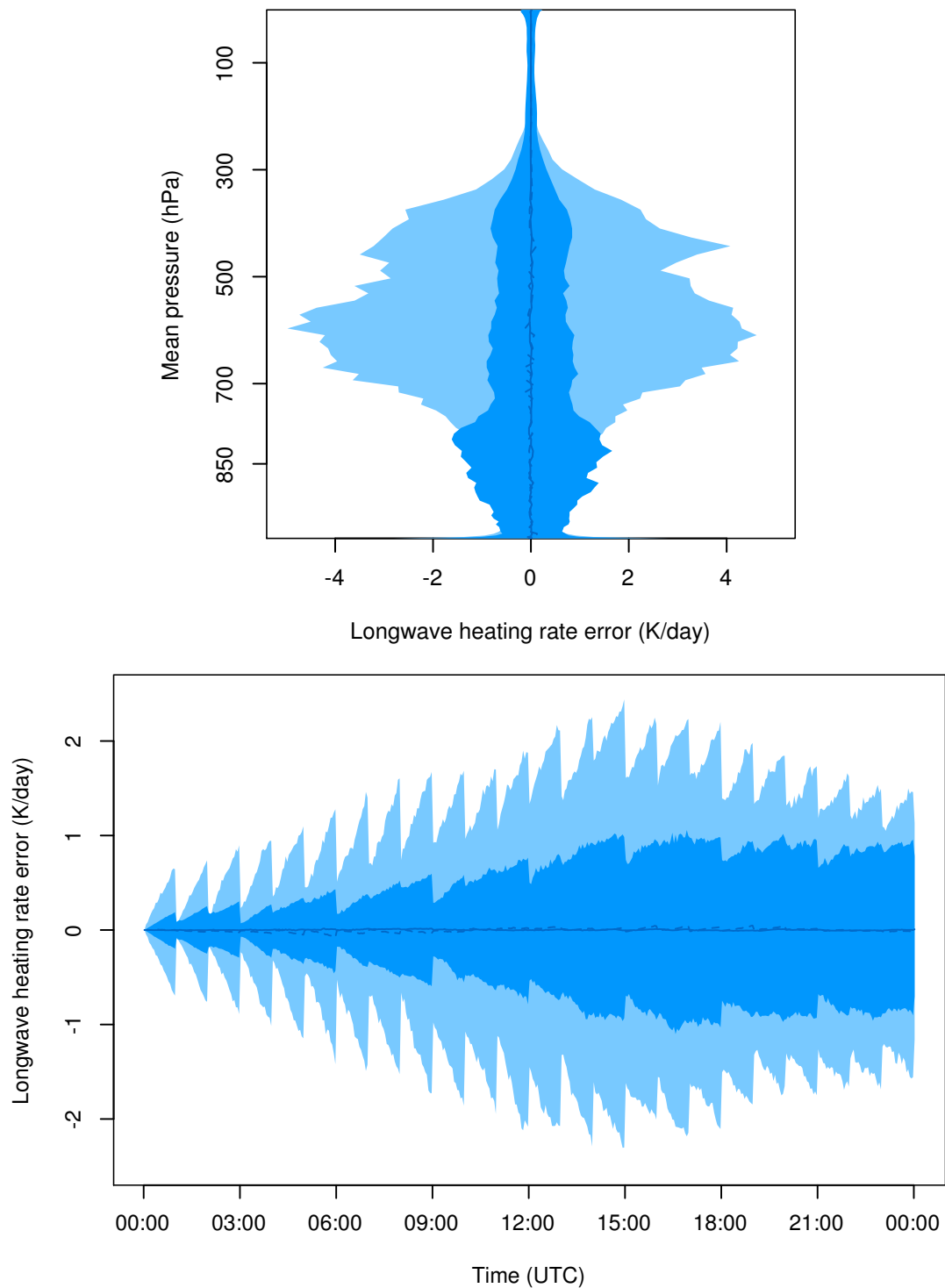
Figure B.1: Impact of intermittency in ACRANEB2 and FMR on longwave heating rate error. Shown is the vertical profile (**top**) and time series (**bottom**) of heating rate error and 90 % confidence bands of 1-h intermittency runs of ACRANEB2 (**darker shade**, **solid line**) and FMR (**lighter shade**, **dashed line**). In the time series plot heating rate error is weighted by pressure thickness of layers (by resampling). The situation is a convective summer day of 29 May 2009 over Central Europe.
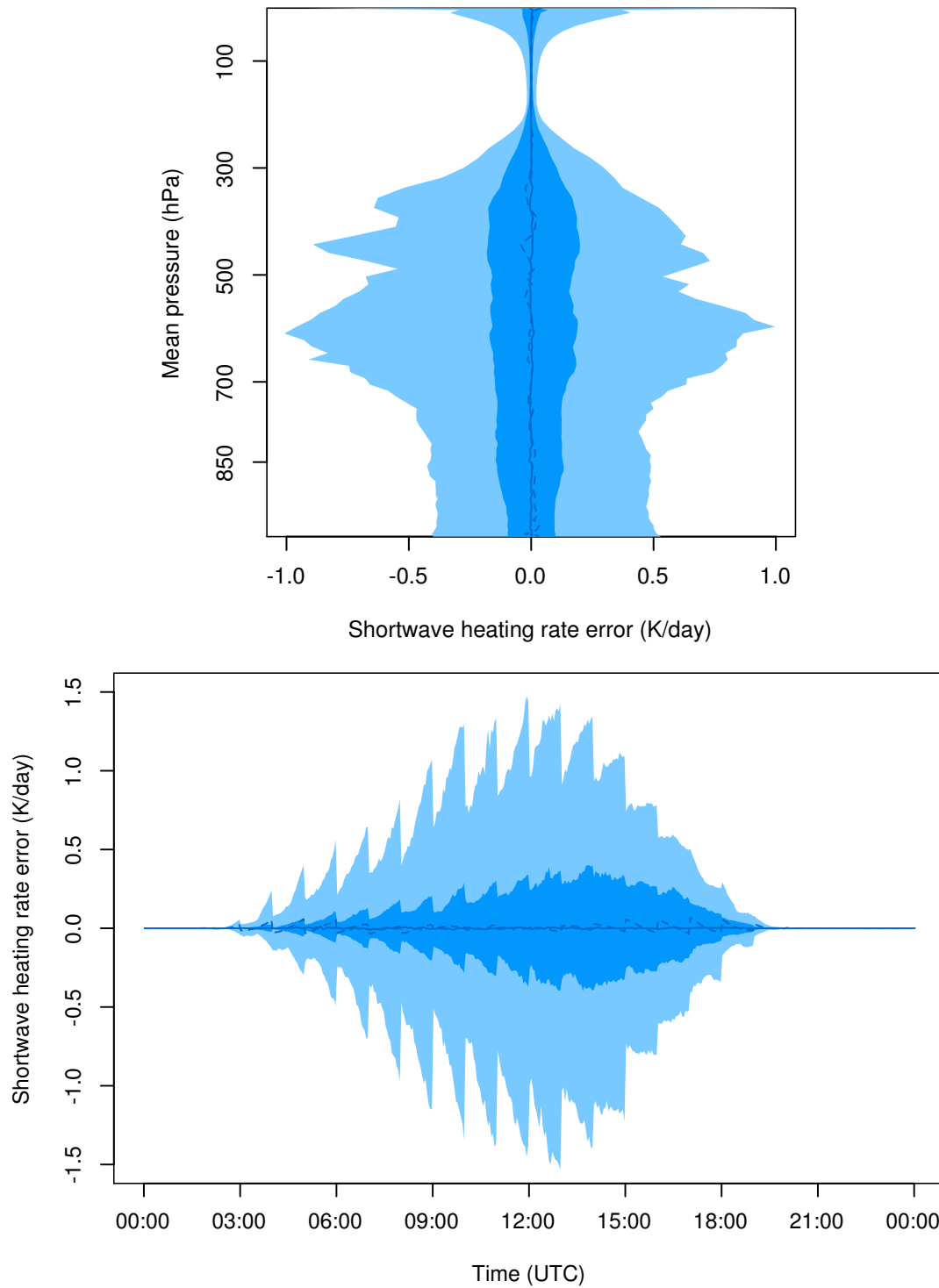
Figure B.2: Impact of intermittency in ACRANEB2 and FMR on shortwave heating rate error. Shown is the vertical profile (**top**) and time series (**bottom**) of heating rate and 90 % confidence bands of 1-h intermittency runs of ACRANEB2 (**darker shade**, **solid line**) and FMR (**lighter shade**, **dashed line**). In the time series plot heating rate error is weighted by pressure thickness of layers (by resampling). The situation is a convective summer day of 29 May 2009 over Central Europe.

Bibliography

Fouquart, Y and B Bonnel (1980). "Computation of solar heating of the Earth's atmosphere: A new parameterization." In: *Contrib. Atmos. Phys.* (53), pp. 35–62.

Geleyn, JF, R Fournier, et al. (2005). "A new 'bracketing' technique for a flexible and economical computation of thermal radiative fluxes, scattering effects included, on the basis the Net Exchanged Rate (NER) formalism". In: *Research Activities in Atmospheric and Oceanic Modelling (Blue Book)*. WMO: CAS/JSC Working Group on Numerical Experimentation. URL: http://www.wcrp-climate.org/WGNE/BlueBook/2005/chapters/04.pdf.

Geleyn, JF and A Hollingsworth (Feb. 1979). "An Economical Analytical Method of the Computation of the Interaction Between Scattering and Line Absorption of Radiation". In: 50.1.

Goody, Richard M and Yuk Ling Yung (1995). *Atmospheric Radiation: Theoretical Basis*. Oxford University Press. ISBN: 978-0195102918.

Liou, Kuo-Nan (2002). *An Introduction to Atmospheric Radiation, Second Edition*. Vol. 84. Academic Press. ISBN: 978-0124514515.

Mašek, J et al. (2014). "Single interval shortwave radiation scheme with parameterized optical saturation and spectral overlaps". In: Manuscript submitted for publication.

Mlawer, EJ et al. (1997). "RRTM, a validated correlated-k model for the longwave". In: *J. Geophys. Res.* (102), pp. , 16, 663–16, 682, 1997.

Mlawer, Eli J et al. (2012). "Development and recent evaluation of the MT_CKD model of continuum absorption". In: *Philosophical Transactions of the Royal Society A: Mathematical, Physical and Engineering Sciences* 370.1968, pp. 2520–2556.

Morcrette, J-J, G Mozdzynski, and M Leutbecher (2008). "A Reduced Radiation Grid for the ECMWF Integrated Forecasting System". In: *Monthly Weather Review* 136. DOI: 10.1175/2008MWR2590.1.

Petty, Grant W. (2006). *A First Course in Atmospheric Radiation, Second Edition*. Sundog Publishing. ISBN: 978-0-9729033-1-8.

Ritter, Bodo and Jean-Francois Geleyn (1992). "A comprehensive radiation scheme for numerical weather prediction models with potential applications in climate simulations". In: *Monthly Weather Review* 120.2, pp. 303–325.

Rothman, Laurence S et al. (2009). "The HITRAN 2008 molecular spectroscopic database". In: *Journal of Quantitative Spectroscopy and Radiative Transfer* 110.9, pp. 533–572.

Serdyuchenko, A et al. (2013). "High spectral resolution ozone absorption cross-sections–Part 1: Measurements, data analysis and comparison with previous measurements around 293 K". In: *Atmospheric Measurement Techniques Discussions* 6.4. Data: `http : / / igaco - o3 . fmi . fi / ACSO / files / cross _ sections / Serdyuchenko / SerdyuchenkoGorshelev5digits . dat`, pp. 6567–6611. URL: `http://www.atmos-meas-tech-discuss.net/6/6567/2013/amtd-6-6567-2013.pdf`.

Solomon, S et al. (1998). "Absorption of solar radiation by water vapor, oxygen, and related collision pairs in the Earth's atmosphere". In: *Journal of Geophysical Research: Atmospheres (1984–2012)* 103.D4, pp. 3847–3858.

Thomas, GE and K Stamnes (2002). *Radiative transfer in the atmosphere and ocean*. Cambridge University Press.

Zdunkowski, Wilford, Thomas Trautmann, and Andreas Bott (2007). *Radiation in the Atmosphere: A Course in Theoretical Meteorology*. Cambridge University Press. ISBN: 978-0-521-87107-5.